METAMATERIAL ENHANCED BROADBAND DIPOLE ANTENNA WITH SELECTIVE DIRECTIVITY AND ENHANCED GAIN

by

Ajay Naik

A thesis submitted to the faculty of
The University of North Carolina at Charlotte
in partial fulfillment of the requirements
for the degree of Master of Science in
Electrical Engineering

Charlotte

2017

Approved by:

_____
Dr. Ryan S Adams

_____
Dr. Thomas P Weldon

_____
Dr. Tao Han

©2017
Ajay Naik
ALL RIGHTS RESERVED

ABSTRACT

AJAY NAIK. Metamaterial Enhanced Broadband Dipole Antenna with Selective Directivity and Enhanced Gain. (Under the direction of DR. RYAN S ADAMS)

This research is aimed at investigating the interaction between a broadband dipole and metamaterials. Metamaterials are artificial electromagnetic structures whose electric permittivity and magnetic permeability can be engineered to have parameter values not available naturally. Metamaterials are popular in modern day research due to their interesting properties. The affect of using metamaterials to alter the directivity of the broadband dipole antenna is the focus of this work. Different metamaterial unit cells have been designed to be used as near field components to achieve selective directivity and improved gain. The antenna and metamaterials are modeled in ANSYS HFSS, a full wave FEM electromagnetic solver. On achieving satisfactory results from the simulation of the bow tie antenna and metamaterial unit cell separately, the process is extended to the design of a bow tie antenna surrounded by a 4x5 array of edge coupled split ring resonators also known as complementary split ring resonators that exhibit negative permeability when excited by the axial magnetic field from the antenna. Unlike, the conventional dipole antenna with omni-directional propagation the new antenna is designed to have directional propagation, and improved gain.

ACKNOWLEDGEMENTS

I would like to take this opportunity to thank all the people for making this Master's a great learning and life experience. I have learnt more in these two and half years than ever, courtesy of my advisor, colleagues and friends. Firstly, in this regard I would like to thank my advisor Dr. Ryan S. Adams for being great mentor all throughout my graduate studies. To briefly describe my graduate school it is courses under Dr. Adams and research under Dr. Adams. I am blessed to be part of electromagnetics lab with best colleagues and friends you could ever have in Dip Thakar, Kathyrn Smith, Arnab and Navneet Yadav. I am especially grateful to my friends, Dip who has been there with me throughout this journey uplifting me when needed and Kathyrn for all the support I got to work my way around in the lab. Finally, I would like to thank my family, my parents Rama and Ramachandra for everything. My sister Shruti and brother-in-law Lokesh for their support. I would also like to appreciate my aunt Geeta and friends Phaneendra, Harinath, Siddu, Santoshkumar and Pradeep B.K for keeping me motivated and supporting me throughout. I am grateful to all the things in my life and would like to thank the almighty for everything I have today.

DEDICATION

To my uncle Sunil,

I am here today and, able do what I am doing because of you. Thank You for your love and support. You will always be in our memories.

TABLE OF CONTENTS

LIST OF FIGURES

LIST OF TABLES

LIST OF ABBREVIATIONS

AMC Artificial Magnetic Conductors

DNG Double Negative Materials

DPS Double Positive Materials

EBG Electromagnetic Band Gap

ECSRR Edge Coupled Split Ring Resonator

ENG Epsilon Negative Materials

FDTD Finite Difference Time Domain

HIS High Impedance Surface

LTE Long Term Evolution

MIMO Multiple Input Multiple Output

MNG Mu Negative Materials

MTM Metamaterials

PBG Photonic Band Gap

RSSI Received Signal Strength Indication

SATCOM Satellite Communication

SRR Split Ring Resonator

TEM Transverse Electromagnetic

WLAN Wireless Local Area Network

CHAPTER 1: INTRODUCTION

The use of radio waves for communication is a common feature in the present day. Almost every electronic device and/or a system utilizes different regions of the electromagnetic spectrum to send and receive data. The Electromagnetic spectrum categorizes waves in terms of their frequency and are assigned bands ranging from Low Frequency(LF) to Tremendously High Frequency(THF) as seen in Fig.1.1. Most of the wireless communication uses radio, microwave and infrared regions of the spectrum and use of higher frequency for communication is the subject of modern day research.

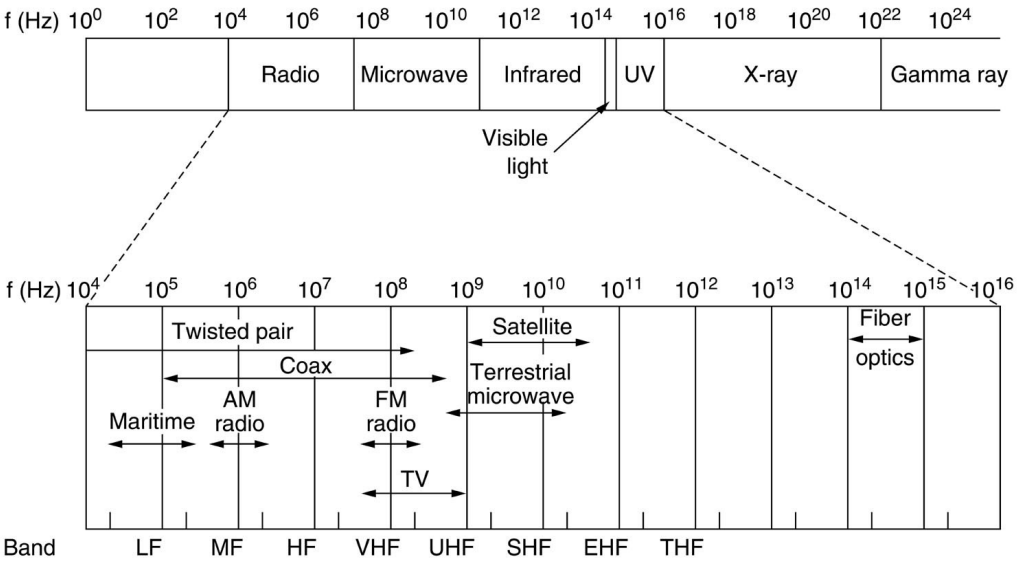

Figure 1.1: Electromagnetic spectrum representing waves in terms of frequency and assigned bands of operation and applications respectively [1].

The primary reasons for the use of wireless communication are that they provide a host of benefits. Mobility, flexibility, easy to install and work with, in addition to being economical compared to their wired counterparts are some of the major reasons for the extensive use of wireless communication. These system advantages have

made them a viable form of communication used for various applications. Some of the important applications include: Mobile Telephone system, Satellite Communication, Radar, Global Positioning System, WLAN, Television and Radio broadcasting, Bluetooth, Radio Frequency Identification, RF Imaging to name a few. All forms of wireless communication uses electromagnetic waves to send and receive information from one point to another. One critical component in wireless communication systems is an antenna. Antennas play a vital role as they are the electromagnetic sensors that can capture and also radiate radio waves to and from air (free space) used in almost all the applications of wireless communication.

Mobile telephony is among one of the major applications of wireless communication and is ubiquitous. The proliferation of mobile telephony has had a significant impact on our lives. Mobile telephony started with 1G which was used for voice communication which was followed by 2G digital wireless technologies with increased voice capacity with increased number of users. The 3G wireless technologies introduced data with voice enabling mobile broadband services and better connectivity. Currently, 4G LTE, is in coexistence with 3.5G and 3.75G other than having more capacity it is faster and provides better mobile broadband experiences [2]. But the growth in the number of users combined with bandwidth limitations, and effects such as fading remain challenges moving forward and have intrigued a large number of researchers and companies to work towards the next generation systems to be deployed in the near future. According to recent data, 70% of youth population spread across 104 countries in the world rely on mobile communications to access the Internet. The number of mobile broadband users has seen a steady rate of increase, 20% annually bringing the total to upwards of 4 billion [3]. The increase in the number directly affects the quality of the service due to the crowding of the spectrum. This results in call drops and communication delays. Today, the technology is in preparation to introduce 5G wireless which addresses the need for higher bandwidth and speeds.

This technology intends to use the unused higher frequency bands, upwards of 28 GHz ,on the electromagnetic spectrum and introduce small cell architectures [4]. As the antenna is the most important system component in radio communication, the advancement in antenna technology would ensure the successful migration to newer technologies. In the next section, the first principles of wireless energy transfer is discussed from a brief historical perspective and a class of materials with properties not found in nature known as metamaterials is introduced as it is a vital topic related to this research.

1.1 Electromagnetics of Antennas and Metamaterials

Maxwell's equations form the fundamental basis of electromagnetics which helps us to understand the electric and magnetic fields in general. Let us consider an ideal electric conductor such as wire, the current flowing through this wire can lead to electrocution and much worse, assuming electromagnetic energy flows inside the wire. An ideal wire acts as a guide of energy than a medium. This concept can be explained in the scenario where RF power is delivered to a load in free space not connected physically by a wire. For this case let us imagine two antennas separated in space as illustrated in the Fig.1.2.

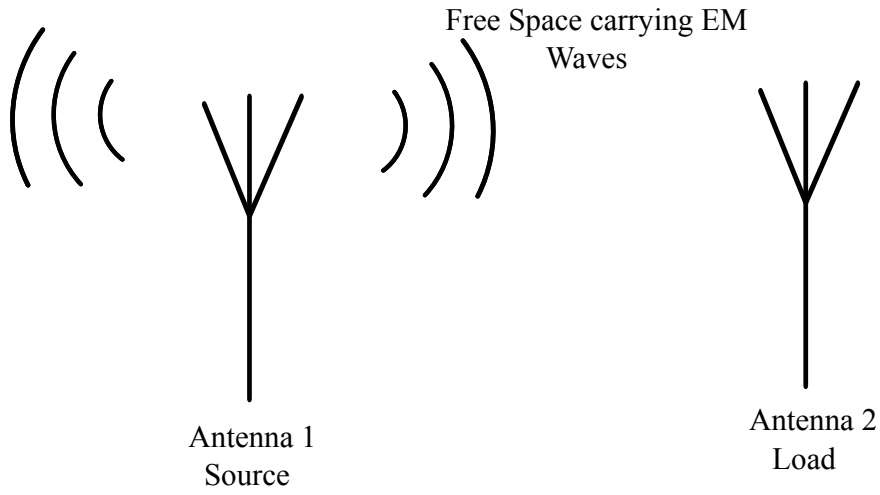

Figure 1.2: Source (Antenna 1) radiates energy into free space the power is contained in time varying Electrical and Magnetic fields received at the Load (Antenna 2) and the total power transferred is given by Poynting's theorem

From Poynting's theorem we know that

$$P = \frac{1}{2} Re(\vec{E} \times \vec{H}^*) \tag{1.1}$$

For real power to be transferred to the load necessary condition is that E and H must be non zero and have the right phase. If either of $\vec{E}$ or $\vec{H}$ is zero or phase difference is quadrature(90°) no real power gets transferred to the load, in the case shown in the Fig. 1.2 the energy has to be transferred from Antenna 1 to Antenna 2 in free space. If either of the two constraints mentioned earlier applies to Antenna 1 referred as source then all the energy is stored with in the source in the form electrical and magnetic energy resulting in no propagation. Therefore, for power transfer from Antenna 1 to Antenna 2 there is a need for dissipation of energy and this is offered by the radiation resistance of antenna. This idea is the fundamental concept governing the antenna design and operation. The other need is the discontinuity to the motion of current through the antenna causing dispersion resulting in propagation. Antennas have evolved from being made of simple wires to complex configurations with materials loaded to influence the performance. More recently, the use of metamaterials

with antennas to enhance fundamental properties is investigated with vigor. These materials are special in a way wherein the $\mathcal{E}$ and the $\mathcal{H}$ with Poynting vector form the left handed triad i,e the phase velocity of the wave and the Poynting vector are anti-parallel to each other and introduced later in this chapter.

Antenna in general is used to transmit and receive radiated waves. It can be operated in transmit or receive configuration or both using a switch. The condition for radiation in a thin wire is described in detail in [7]. The conclusion drawn from this is that the effect of radiation in a conductor is caused by accelerating charges or dispersion of currents. This consequence has enabled the design of various types of antennas and is the fundamental principle governing the operation of an antenna. Some forms of common antenna types are: wire antennas, aperture antennas, microstrip antennas, array antennas, reflector antennas, lens antennas etc., more information of these can be found in [7] and [8]. From an historical standpoint it might be helpful to note that antennas concepts were used to provide the experimental proof for Maxwell?s equations. The first wireless system developed to verify Maxwell?s equations was demonstrated in 1886 was by Henrich Hertz at Technische Hochschule in Karlsruhe. Henrich Hertz was the former pupil of Herman Von Helmholtz who in 1879 sponsored a prize for experimental validation of Maxwell?s theory. Oliver Lodge, then physics professor at University College of Liverpool also published his own confirmation a month after Hertz [9].

The first wireless transmission was demonstrated by Marconi in 1901 using a 152.4 meter kit-supported antenna this ushered the era of antenna technology. Even though others had conducted similar experiments this remains a genesis of antenna era. Tesla and Noble studied use of radio waves for power transmission. In 1920 Yagi Uda antenna was introduced which consisted of dipole with parasitic elements. It is one of the most popular used as TV antennas and remains relevant to date. In the decades that followed especially 1940s renewed interest in microwave antenna technology leading

to the development of waveguides, horns and reflectors. These antennas were further used by agencies such as NASA for astronomy, deep space communications and SATCOM systems. H. A. Wheeler introduced the concept of small antennas and radian sphere containing the radiated energy. Chu and others followed his lead to come up with the fundamental limitations on electrically small antenna. Small antennas exhibit high Q implying a inverse relationship between bandwidth and gain. The knowledge of which led to the development of fractal antennas where the quality factor (Q) of the radiating element is decreased. Following decades i.e, 1950s and 1960s saw the development of helical antenna by Kraus and introduction of frequency independent antennas by Rumsey. Microstrip patch antennas came into existence in 1970s and have remained primary choice for most modern day applications due to their versatility and low profile. The integration of materials to optimize the performance of the antenna has been a common feature in 1990s and 2000s with the introduction of metamaterials which captured the imagination of industry and academics. The advancement in wireless communication technologies have propelled the development of Multiple Input Multiple Output(MIMO) and reconfigurable antennas. Artificial impedance surfaces such as high impedance surface(HIS), Electromagnetic Band gap (EBG) and Artificial Magnetic Conductors (AMC) are commonly found as part of the antennas providing interesting characteristics [10]. This work derives inspiration from the recent developments in antennas technology, metamaterials and the interactions of both in particular.

Antenna performance is determined by design metrics known as antenna parameters. They are mathematical models that can be generated using full wave simulators to obtain desired results and validate the design. The important antenna parameters relevant to this work are:

1. Radiation Intensity : "The power radiated from an antenna per unit solid an-

gle." It is a far field parameter and given as

$$U = r^2 W_{rad} \tag{1.2}$$

where U is the radiation intensity in Watts/unit solid angle and W_{rad} is the radiation density in Watts/m^2.

2. Directivity: "Ratio of the radiation intensity in a given direction from the antenna to radiation intensity averaged over all directions".

$$D = \frac{4\pi U}{P_{rad}} \tag{1.3}$$

where U is the radiation intensity with units Watt/unit solid angle and P_{rad} is total radiated power in Watts (W).

3. Gain: "Ratio of the intensity in a given direction to the radiation intensity that would be obtained if the power accepted by the antenna was radiated isotropically."

$$G = 4\pi \frac{U(\theta, \phi)}{P_{in}} \tag{1.4}$$

P_{in} is total input power in Watts. Gain is also the measure of efficiency of the antenna combined with directional ability of the antenna hence remains an important figure of merit for a design.

4. Antenna Polarization: Antenna polarization refers to the polarization of the wave radiated from an antenna. Generally, the orientation of the time varying instantaneous electric field observed from a fixed point is used to determine the polarization. A fully polarized wave, in general, takes the shape of an ellipse. The special cases of elliptical polarization that are commonly seen in antennas are linear and circular respectively. Linear can be further categorized

as horizontal and vertical, and the circular polarization can be distinguished as being right hand circularly polarized or left-hand circularly polarized.

Gain and directivity are used to classify antennas as omni-directional and directional antennas. Omni-directional antenna radiate energy 360° horizontally. They are used when the coverage is required in all direction (horizontally) from antenna with varying degrees of vertical coverage. On contrary, directional antenna have increased directivity and gain in one direction compared to the others. The need for directional antennas in the age of satellite communication and advancement of wireless communication is of importance. For example, directional antennas find their use in environments effected by reflection, refraction or diffraction. Chu expressed the limitation on linear polarized electrically small antenna with respect to bandwidth, size and gain. Harrington extended the work to circularly polarized antennas. These studies pose a limit on the size of the antenna to achieve maximum gain and bandwidth. However, the introduction of non-foster circuit to match antenna impedance has proved to be a way to overcome this limitation [5].

The topic of metamaterials has been one of the newest additions to field of electromagnetics. Metamaterials are artifical materials whose permittivity and permeability, dispersion relationship can be engineered to provide values not available in nature. This degree of freedom in material synthesis has led to new antenna configurations using metamaterials pushing the envelop further in antenna technology. The benefits of metamaterials are: small physical size, low cost broad bandwidth, good efficiency. They are used to change the boundary conditions in the near field of the antennas. This has led to the genesis of new class of antennas known as metamaterial-based small antennas. They are further classified into four categories:

1. CRLH base or dispersion engineered resonant antennas. These are antennas with negative-order modes and zeroth-order resonators.

2. Small antennas with negative epsilon and negative mu loading .

3. Metaresonator antennas based on split ring resonators and complementary split ring resonators.

4. Antennas loaded with metasurfaces.

All known materials follow the right hand propagation i.e, the Poynting vector and the phase velocity are parallel to each other. However,this relation for the metamaterials is other way around. The existence of such materials was first conceptualized by Vesalago in 1964. In his seminal paper, materials with simultaneous negative values of permittivity and permeability are discussed and their possible implications on wave propagation is presented [6]. It took nearly thirty years, after this paper to develop first material of the kind discussed by Vesalago [7]. Since then metamaterials have been generated a lot of excitement and research in the field of electromagnetics and antenna technology has also benefited from their discovery. Various antenna designs centered around the use of metamaterials to alter the fundamental properties of metamterials have been experimented by various research groups leading to interesting results. The next section discusses objective followed by related work, and finally the structure of the thesis.

1.2 Objective of the Thesis

As described earlier the accessibility and ease of wireless and satellite communication has resulted in the increase in number of users. Antenna systems have played a vital role in this progress and remain critical component in future systems. However, with the increasing demands on technology more than ever before has created a scope for new and innovative antenna designs with economical benefits associated with scaling of the system. In the applications such as in satellite communication and navigation, antennas rely on complex algorithms and hardware equally to solve the problems associated higher bandwidth, gain which translates into better quality

of service, mitigation of interference and multipath fading. Omni-directional antenna have their usefulness in applications such as mobile handsets however, on the same note directional antennas find themselves suited for applications such as indoor wireless networks. The next generation wireless communication systems, satellite communication terminals and novel applications such as RF imaging using RSSI benefit from the use of directional antenna. A phased array antenna or a smart antenna is used in the design of directional antenna. However, this option affects the cost and size of the overall system for a given frequency. In this regard, the novel antenna designs with metamaterials and their economic benefits are taken into consideration to design a directional antenna which is the primary objective of this work. The goals of the thesis are first to understand broadband dipole antennas and metamaterials, with focus on the study of electromagnetic interactions between the metamaterial and the antenna. Secondly, to design different antenna configurations by loading antenna with metamaterials and once satisfactory results are obtained an attempt is made to design, simulate and fabricate antenna configurations to obtain selective directivity and enhanced gain.

1.3 Related Work

In this section we review some of the important papers leading to the work this thesis plans on doing. Brown, Parker and Yablonovitch used photonic crystal substrate to investigate the radiation properties of a bow tie antenna. Photonic band gap (PBG) structures inhibit propagation in the band gap region and are easier to fabricate at microwave frequencies. Two different measurements were made one involving a bow-tie antenna on a PBG substrate and the other with antenna on Stycast substrate with same dielectric constant and thickness as the solid portion of the photonic crystal. The results of these measurements showed no radiation of waves in the PBG substrate when operated in the band gap region. On contrary, antenna on the Stycast substrate with the same frequency had multiple lobes. The conclusion that

can be drawn is PBG crystals suppressed the surface waves and hence increased the efficiency of the antenna [8]. This has been the basis for works that followed. One work in particular done by Dadgarpour and colleagues increased the performance of a Yagi-Uda type end-fire-bow-tie antenna configuration loaded with a 2x5 array of enhanced end-coupled-split-ring (EECSR). Significant increase in the gain is found with antenna loaded with EECSR structure and increasing the number of EECSR arrays results in better gain [9]. The antenna itself has three elements and an array of such a configuration is much larger than one this work proposes. Enoch and colleagues showed that directivity of point source inside metameterials consisting of metallic mesh of thin wires operated at frequency on the edge of the band gap, as in PBG, behaved like a negative epsilon medium which resulted in the enhancement of directivity of the source. The source in the experimental setup was a monopole surrounded by metamaterials and this resulted in the controlled emission of electromagnetic radiation [10]. Furthermore, Wu, Wang and others at MIT also published work on the interaction of antenna with metamaterial resulted in better directivity. The study investigated various periodic collections such as thin wire, rings and these were used as substrate for a dipole antenna. The radiation properties of the substrate were altered and detailed analysis is presented [11]. Ziolkowski used metamaterials to enhance the directivity of electrically small antennas involving end-fire two element dipole. The operating frequency for this work is in the range of MHz whereas, the topic of this research seeks to accomplish similar feat at higher frequency where the design of can be challenging due to smaller size of the metamaterials [12]. In summary for this work, the advantages of metamaterial loaded antenna are considered to control the far field radiation properties and to propose way/s to achieve selectivity in directivity and improved gain as done some of the work presented above.

1.4 Structure of the Thesis

The thesis is organized as follows, first chapter presented the context, problem statement, related work and motivation to pursue a specific approach to solve the problem.

The second chapter examines, the most basic yet ubiquitous, dipole antennas. The parameters such as far fields radiation characteristics of common antenna types are presented with necessary equations. The chapter explains the choice of bow tie antenna used in this work.

The third chapter introduces a characterization of materials,metamaterials, brief history of the same. It explores different unit cell structures, address differences between metamaterials and metasurfaces. The aim of the chapter is to explain the use of split ring resonators (SRR),the preferred unit cell structure for this work.

The fourth chapter integrates the concepts derived from chapters three and four to design, simulate and fabricate the proposed antenna meeting the requirements. It summarizes simulated and measured results with a detailed discussion.

Finally, conclusion succinctly expresses the overall work, its significance and further study that would benefit the in taking this work forward.

CHAPTER 2: BROADBAND DIPOLE ANTENNAS

Dipole antennas, the name directly follows from the number of radiating elements involved in transfer and reception of energy to and from free space. A dipole has two conductors fed by signal with 180° phase difference between the two guides acting as the antenna. The advantages of these antennas are the design procedure is simple and can be made using thin wires. The basic analysis of thin wire dipoles forms a strong foundational background of antenna theory. Hence in this chapter, a discussion on various types of dipoles and their field equations are presented, compared and the analysis is further extended to broadband counterparts such as bi-conical and bow tie (bi-fin) antennas to make a qualitative choice of the antenna to be used to solve the problem of directional propagation.

2.1 Thin Wire Dipoles

Dipoles are categorized based on how their overall length relates to the wavelength. An infinitesimal dipole can be seen as a linear wire whose length is much smaller than the wavelength of operation($l << \lambda$) is very thin i.e., thickness($t << \lambda$). A mathematically complete analysis can be found in [13]. A thin wire dipole analysis is based on constant current distribution in the wire due to its dimensions. The electric and magnetic field in the far field of the infinitesimal dipole is given as

$$H_\phi = \frac{jkI_0 l \sin\theta}{4\pi r}\left[1 + \frac{1}{jkr}\right]\exp^{-jkr} \tag{2.1}$$

$$E_r = \eta\frac{I_0 l cos\theta}{2\pi r^2}\left[1 + \frac{1}{jkr}\right]\exp^{-jkr} \tag{2.2}$$

$$E_\theta = j\eta \frac{kI_0 l sin\theta}{4\pi r}\left[1 + \frac{1}{jkr} - \frac{1}{(kr)^2}\right]\exp^{-jkr} \tag{2.3}$$

where k represents the propagation constant and r radial distance. The remaining field components $H_r = H_\theta = E_\phi = 0$. The other fundamental parameter in antenna is radiation resistance R_r, for infinitesimal dipole

$$R_r = 80\pi^2\left(\frac{l}{\lambda}\right)^2 \tag{2.4}$$

Thin wire dipoles are not practical but they can be used to characterize capacitor-plate antennas, inverted T and inverted F antennas.

A realizable version of the dipole is a small dipole antenna ($\frac{\lambda}{50} < l < \frac{\lambda}{10}$). The field equation for this antenna for $kr \gg 1$ is given by

$$E_\theta \approx j\eta \frac{kI_0 l \exp^{-jkr}}{8\pi r} sin\theta \tag{2.5}$$

$$H_\phi \approx j sin\theta \frac{kI_0 l \exp^{-jkr}}{8\pi r} \tag{2.6}$$

The next iteration of a dipole antenna is the finite length dipole with length ranging in between $\lambda/2$ and $\lambda/2 < l < \lambda$. The far field equations for this dipole has similar components of electric and magnetic fields multiplied by an additional space factor. This space factor useful in the design of arrays.

$$E_\theta \approx j\eta \frac{I_0 \exp^{-jkr}}{2\pi r}\left[\frac{cos(\frac{kl}{2}cos\theta) - cos(\frac{kl}{2})}{sin\theta}\right] \tag{2.7}$$

$$H_\phi \approx j \frac{I_0 \exp^{-jkr}}{2\pi r}\left[\frac{cos(\frac{kl}{2}cos\theta) - cos(\frac{kl}{2})}{sin\theta}\right] \tag{2.8}$$

From the above equations the first observation that can be drawn is that the radiation is broadside implying the fields are maximum when $\theta = 90^\circ$ fields go to zero when $\theta = 0^\circ$. The second observation is the far field radiation pattern is due

to E_θ and H_ϕ and the enhancement or suppression of these components alter the radiation characteristics of the antenna. The dipole antennas are resonant structures as their radiation characteristics are depend on the length of the overall antenna. This effects their operation and limits it to a narrowband. For a half wavelength dipole small changes in length has a strong affect on the reactance of the antenna. Furthermore, the imaginary part of the antenna impedance can be moved back and forth as a function of frequency by inducing small changes in antenna length. The feeding mechanism for a wire dipole requires balun in order to reduce reflections and transfer all the energy from the source to the antenna. This problem is circumvented, if the thickness of the wire is increased consequently offering wider bandwidth. These points are taken into consideration and the study is extended to broadband dipoles which meet the conditions specified in the previous line.

2.2 Biconical Antenna

The practical realization of a broadband dipole requires increasing the thickness of the wire. This change gives rise to currents in the direction perpendicular to the wire and hamper the overall gain of the antenna. Also, for improved bandwidth it is important for the antenna geometry enclosed inside a sphere of radius r, to utilize the volume of the sphere efficiently. This can be accomplished by the use configurations with larger volumes such as cones, hemispheres, tapers geometries. In this regard, though hemisphere has wider bandwidth compared to taper and conical antenna types they are not preferred for this work. The reason for this choice is due to need for space to incorporate metamaterials within the sphere containing the antenna volume, difficulty in fabrication and mechanical assembly. Therefore, conical configurations are investigated further as tapers and cones share the same bandwidths. Among the antennas made of cones, conventional bi-conical antenna which is made up of two cones is studied. A truncated bi-conical antenna is shown in Fig.2.1. In an ideal case the cones extend up to infinity.

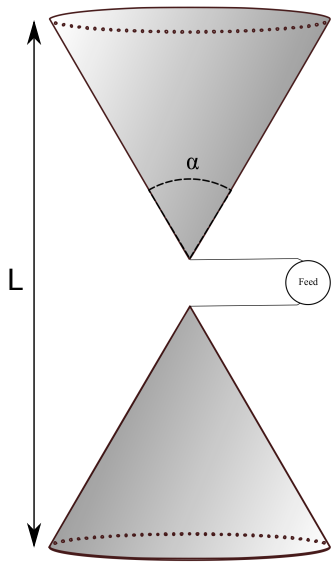

Figure 2.1: Bi-conical Antenna with with feed between two radiating cones and flare angle α and length $L = \lambda/2$.

The far field equations for this antennas are calculated using the following assumptions [14]:

- Cones extend up to $\pm\infty$
- TEM waves are generated by the antenna

The electric and magnetic fields can be derived by using mathematical approach used to derive fields of thin wire dipoles. This results in

$$H_\phi = \frac{H_0}{sin\theta}\frac{exp^{-jkr}}{r} \tag{2.9}$$

$$E_\theta = \eta\frac{H_0}{sin\theta}\frac{exp^{-jkr}}{r} \tag{2.10}$$

Using the assumptions made earlier and the Equivalence theorem the current and the voltage between cones of the antenna is found to be

$$I(r) = 2\pi H_0 \exp^{-jkr} \tag{2.11}$$

$$V(r) = 2\eta H_0 \ln[cot(\frac{\alpha}{4})] \tag{2.12}$$

Setting $r = 0$ and taking the ratio of voltage by current we find the input resistance

$$R_{in} = 120 \ln[cot(\frac{\alpha}{4})] \tag{2.13}$$

The resistance can be arbitrarily chosen by the choice of α. [15] Infinite bi-conical antennas are not practical however, the analysis serves as a starting point to look into practical variants of this antenna including finite bi-conical, bow tie, discone etc. It is useful to know that

- Truncation of the infinite structure leads to higher order modes. This means current on the cones may not be radially directed causing reflections distorting the pattern.
- Larger cone angles reduce the effects of truncation.
- Bandwidth is defined for cone lengths between $\lambda/4 \leq l \leq \lambda/2$

Though bi-conical antenna has attractive radiation characteristics, it is hard to work with mechanically as it can be very large and require supporting structures to hold the cones. Emphasizing on the point made at the beginning of this chapter such a structure would make it difficult to use metameterials around the it. A discone antenna not shown here is similar to bi-conical antenna with one of the cones replaced by a circular metal plate which acts as a ground plane. The dis-cone antenna also imposes the same mechanical constraints hence not used for the design. So a geometrical approximations of conical structure while preserving the radiation characteristics is sought. The search resulted in triangular sheet and bow tie antenna. A bow tie antenna in particular can be constructed using two triangular metal sheet or fabricated on a substrate. This ease in use makes bow tie antenna an ideal choice for this work.

However, the trade off is that bow tie antenna have a narrower bandwidth compared to a bi-conical antenna but significantly larger compared to thin wire dipoles.

2.3 Bow Tie Antenna

A Bow Tie antenna is the planar slice of the bi-conical antenna. The design and the analysis remain the same. The triangular sheet antenna whose structure is equivalent to the bow tie antenna was experimentally investigated by Brown and Woodward [16]. A wire simulation of the antenna significantly reduces weight and wind resistance of the structure. The wire bow tie has narrow bandwidth compared to a triangular sheet antenna and a bi-conical surface. Therefore, the wire version of the antenna is not used here and compactness of the bow tie is an added advantage, if the antenna were to be loaded with materials or near field components.

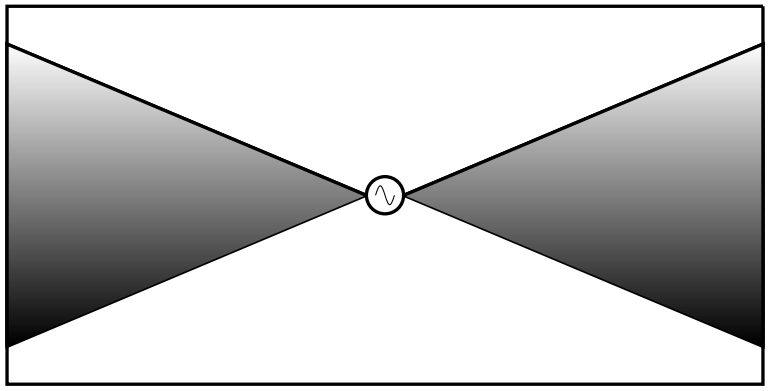

Figure 2.2: A Bow Tie Antenna with feed at the center

From the design perspective, as the flare angle increases secondary lobes become prominent. For electrical length equal to 180° no side lobe appears and for electrical length of 140° the reactance is independent of flare angle. These points are taken into consideration during the design process. A spherical cap, as seen in Fig.2.3, on the triangular shape does not affect the impedance of the antenna even though it effectively increases the antenna length by δ.

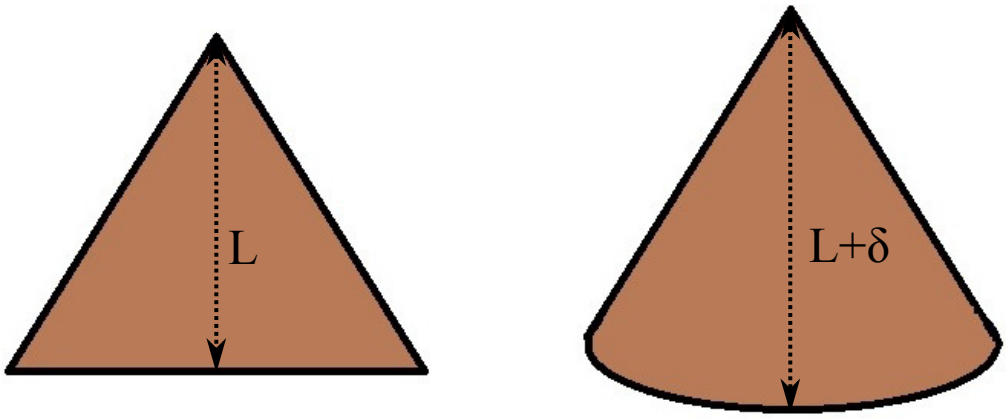

Figure 2.3: The triangular sheet of length L is presented to the left followed by a triangular sheet with a spherical cap having an effective length increased by δ

The feed of the antenna is of equal importance in the design. Since the bow tie antenna is intended to be fabricated on a substrate gives us multiple choices for the feed. Coaxial feed, microstrip line feed and co-planar stripline feeds are commonly used deliver power to a bow tie antenna. Coaxial feed is preferred over others due as to avoid unwanted coupling and fringing effects. Also in case of a microstrip feed the need for the ground plane means the requirement of more metal and with the presence of near field components it is not ideal to have a ground plane as it can lead to a short especially when the dimensions get smaller as the frequency increases. Finally, the advantage of being light and less costly makes bow tie the antenna for the proposed solution.

2.4 Polarization of Broadband Dipoles

Antenna polarization is an important metric to take into consideration. It is a far field parameter and dictates the electrical performance of the antenna directly affecting the gain of the antenna. When the direction is not stated the polarization of the antenna refers to the polarization in the direction of maximum gain. It is

generally considered in context of time varying direction and relative magnitude of the electric-field vector.

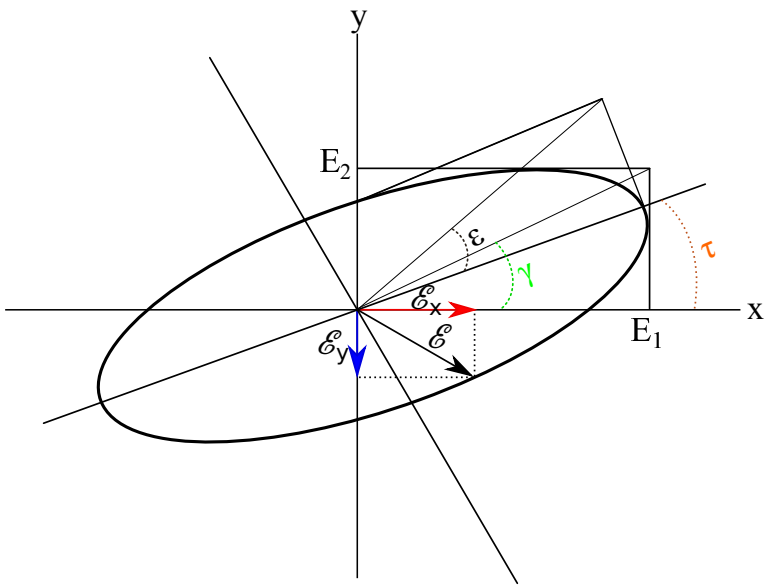

Figure 2.4: General Ellipse traced out by the tip of electric-field $\mathcal{E}$ with the wave travelling in +z direction out of the page.

Fig. 2.4 shows a general ellipse with instantaneous electric field vector $\mathcal{E}$. $\mathcal{E}_x$ and $\mathcal{E}_y$ represent the components in x and y direction respectively. E_1 and E_2 represent the peak values of these components. We have γ describing E_1 and E_2 as

$$\gamma = \arctan \frac{E_2}{E_1} \tag{2.14}$$

where, $0^\circ \leq \gamma \leq 90^\circ$. The tilt angle of the ellipse τ is the angle between the x-axis and the major axis of the ellipse as shown. The angle ϵ is expressed as

$$\epsilon = \cot^{-1}(-AR) \tag{2.15}$$

where, $1 \leq |AR| \leq \infty$ and $-45^\circ \leq \epsilon \leq 45^\circ$, AR being the axial ratio of the ellipse corresponds to the ratio of the major axis electric field component to that along the minor axis. The sign of AR is positive for right-handed ellipse and negative for left-

hand sense. AR is often expressed in dB as $20log|AR|$. The instantaneous electric field for the wave can be expressed as

$$\mathcal{E} = \mathcal{E}_x\hat{x} + \mathcal{E}_y\hat{y} \tag{2.16}$$

which in turn for simplicity can be represented as

$$\mathcal{E} = E_1 \cos\omega t\hat{x} + E_1 \cos(\omega t + \delta)\hat{y} \tag{2.17}$$

where δ is the phase by which the y-component leads the x-component. This representation describes ellipse shape as time t progresses. If the components are in-phase ($\delta = 0$) resulting in linear polarization of the net vector. The orientation of the linear polarization depends on the relative values of E_1 and E_2. If $E_1 = 0$, the polarization is vertical linear and $E_2 = 0$ results in horizontal linear polarization of the wave. This implies that for a linear polarization axial ratio is infinite. In addition, if δ is non-zero, the axial ratio is finite. For positive values of δ the sense of rotation is left-hand with components in-phase and for negative values of δ the components are out of phase and the sense is right-hand. A special case arises when $E_1 = E_2$, circular polarization. The axial ratio in dB for a circularly polarized wave is equal to zero. γ and δ completely specify polarization state of the wave. Either of the two pairs of angles (ϵ,τ) or (γ,δ) uniquely define the polarization state of a wave. The transformations between these angles are given as

$$\gamma = \frac{1}{2}\cos^{-1}(\cos 2\epsilon \cos 2\tau) \tag{2.18}$$

$$\delta = \arctan\left(\frac{\tan 2\epsilon}{\sin 2\tau}\right) \tag{2.19}$$

A linear current carrying element like the thin wire dipole has the wave polarized

linearly. In transmitting mode, the bi-conical antenna and others discussed in this chapter are linearly polarized. The value of axial ratio for practical realizations is expected to be in the order of hundreds of dBs. The metamaterial loading on antenna does not affect the polarization as polarization is a far field parameter and the interaction between the antenna and metamaterial is confined to the near field.

CHAPTER 3: THEORY OF METAMATERIALS

The word metamaterial is used to refer to everything from engineered textured surfaces, artificial impedance surfaces, artificial magnetic conductors, double negative materials, frequency selective surfaces, Photonic Band-Gap (PBG) surfaces, Electromagnetic Band-Gap (EBG) surfaces and even fractals or chirals. In this chapter a brief history is presented followed by theory governing the behavior metamaterials (MTMs) and concluded with a discussion on Split Ring Resonators (SRR).

3.1 Characterization of Media

Electromagnetically materials are classified into four different categories based on their constitutive parameters ϵ (permittivity) and μ(permeability) namely:

- Negative ϵ and positive μ also known as ENG(epsilon negative) material.
- Positive ϵ and positive μ also known as DPS(double positive) material.
- Negative ϵ and negative μ also known as DNG (double negative) material.
- Positive ϵ and negative μ also known as MNG (mu negative) material.

Materials are also characterized based on their behavior when subjected to electromagnetic fields. In linear materials the constitutive parameters are not functions of the applied field. If the constitutive parameter vary with the applied field they are referred to as non linear materials. If the constitutive parameters does not vary with position, on the material, such a material is said to be homogeneous, otherwise inhomogeneous. Inhomogeneity is common feature of most materials however, since it is limited to a small part, the material behavior can be effectively taken to be homogeneous. If the constitutive parameters are the function of frequency they are said

to be dispersive; otherwise non-dispersive. Anisotropic materials are those materials whose constitutive parameters are a function of direction of applied field; if not they are said to be isotropic. For anisotropic materials permittivity/permeability is represented in the form a 3x3 tensor known as permittivity tensor/permeability tensor. Adding to this is another class of materials known as bi-anisotropic materials; they have special property of rotating the polarization of an incident wave. Many double negative materials (DNG) fall under this category. Double Negative materials have are known to exhibit interesting properties such as backward wave propagation and have been used in various applications such as cloaking, design of electrically small antennas, increase performance of lenses, microwave circuits, transmission lines, antennas, photonic crystals and miniaturization [17].

Metamaterials in general sense, are artificially effective homogeneous electromagnetic structures with unusual material properties. The effective homogeneity is due to the presence of smaller unit cells of size a with the constraint that $a << \lambda_g$, where λ_g stands for guided wavelength. This is a necessary condition for refractive index to dominate over scattering and diffraction effects and such a material has constitutive properties. An example of a unit cell is shown in the Fig. 3.1. In general, a unit cell consists of inhomogeneity in the host medium that can be practically realized as a metal on a substrate of a particular geometry. These inhomogeneities are often referred to as meta-particles. The meta-particles behave as atoms in an actual material and are responsible for the electromagnetic properties when appropriate polarization conditions are met. These meta-particles can either have a resonant or non-resonant response to an applied field in general. These meta-particles also known as unit cells are distributed on a substrate. The anisotropic behavior is due to the need for excitation in the proper direction if not they behave as normal materials governed by a right handed relationship between the Poynting vector and phase velocity. Infinitely long thin wires, split ring resonators are some example of unit cells.

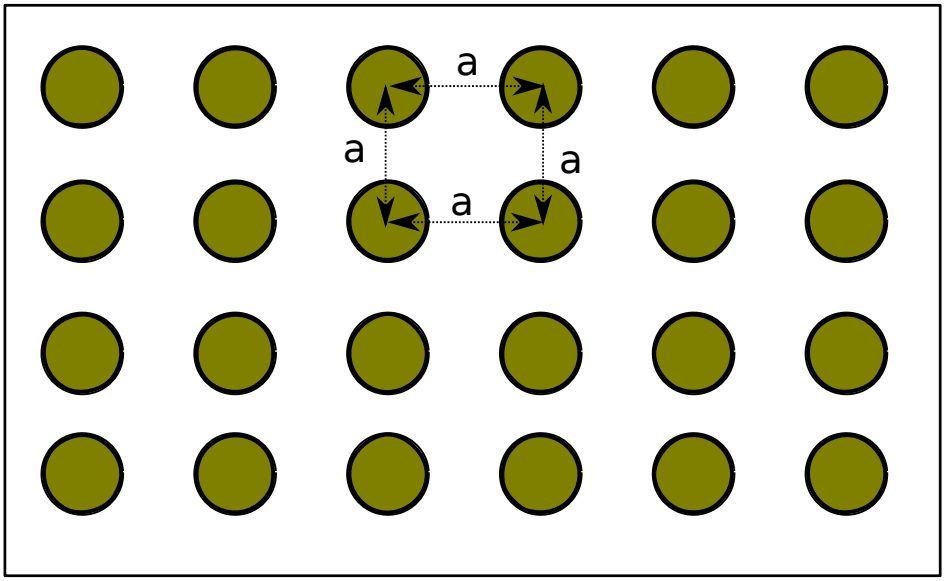

Figure 3.1: An illustration of a metamaterial array consisting of periodically distributed structure with spaced a units apart.

3.2 Historical Overview

The first speculation about electromagnetics of left handed media backward wave propagation and its characterization in using negative refractive index was made by Russian physicist Victor Veselago. In his 1967 paper published in Russian, and later translated in english the following year, concluded that left handed media is allowed by Maxwell's equations. The hypothesized materials with simultaneous negative ϵ and μ would result in interesting phenomena. Among which one conclusion is a LH media could be characterized by NRI and this would allow for the reversal of Snell's law, Doppler effect and Vavilov-Cerenkov radiation [6]. However, no LH material was discovered at the time. It took thirty years for the first practical realization of LH media. Fig.3.2 illustrates backward wave propagation in terms of electric and magnetic field represented as 'E' and 'H', Poynting vector 'S' and phase velocity 'k'. The direction of 'k' and 'S' differ for DPS and DNG, 'S' is given by

$$S = \frac{1}{2} Re(E \times H^*) = \hat{a} S_z \tag{3.1}$$

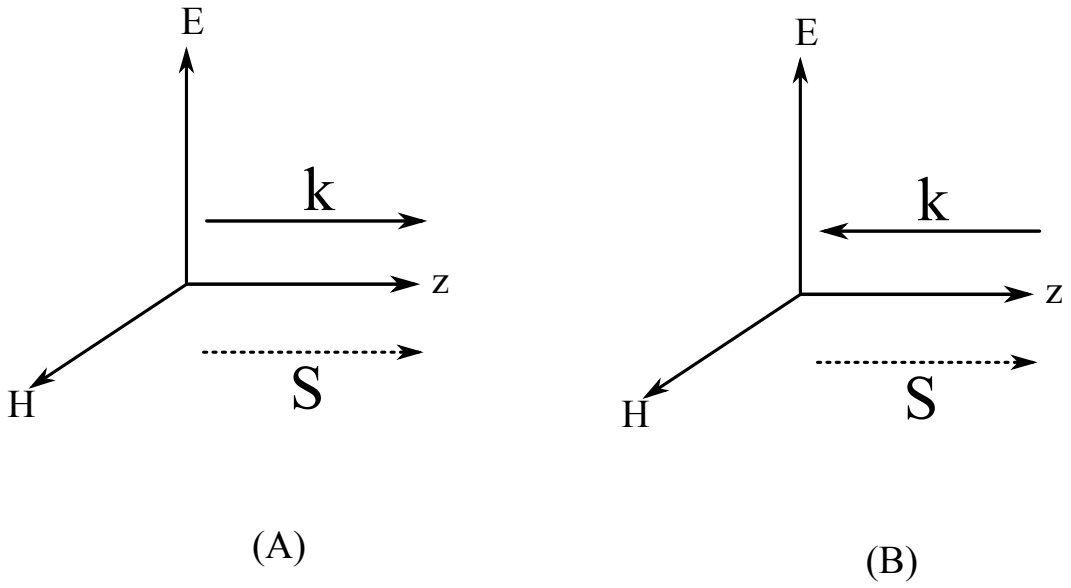

Figure 3.2: (A) Right-Handed propagation with phase velocity in the direction of Poynting vector.(B) Left-Handed propagation with phase velocity anti-parallel to Poynting vector.

Sir J.B.Pendry et. al of Imperial College, London presented microstructures built from nonmagnetic conducting sheets with μ_{eff} tunable to values not accessible in nature. David R. Smith and colleagues at UCSD demonstrated the first experimental proof of negative refractive index (NRI). This spurred great excitement which led to various investigations such as numerical FDTD done by Ziolkowski et al. [18], numerical FEM by Caloz.[19], theoretical EM by Lindell and team [20], Kong and colleagues [21], Smith et al. [22], McCall and team [23] and transfer matrix algorithm approach by [24] amongst others. The field of MTM also attracted criticism and controversy [25, 26, 27, 28] later shown to be based on physics misconceptions. Experimental and numerical techniques such as FDTD simulations have validated the notion of negative values of constitutive parameters and DNG behavior. Experiments at optical frequencies are also carried out which has validated the theory behind such behavior. It is also important to know that metamaterials are not yet found in nature. Therefore, the idea finding one with LH characteristics cannot be disregarded.

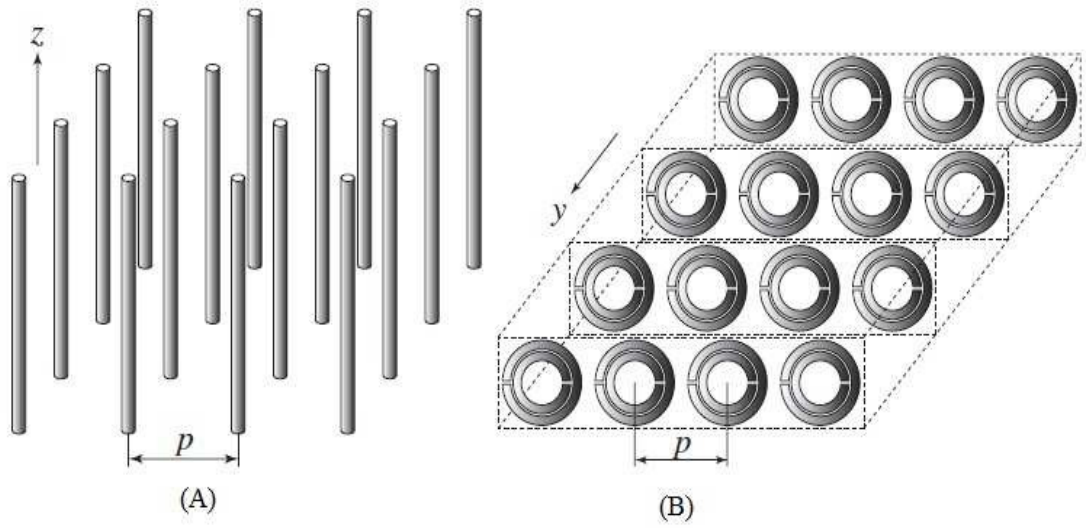

Figure 3.3: Negative- ϵ and negative- μ structures proposed by Pendry. (A) Thin-wire(TW) structure exhibiting negative- ϵ if $E \parallel z$ (B) Split-ring resonator (SRR) structure exhibiting negative- μ if $H \perp y$ [19]

As cited earlier the experiment proof of NRI consisted of split ring resonators were used combined with thin wires. The structures are shown in Fig. 3.3. They can be designed to have their plasmonic frequency, the frequency at which dipole moments mirroring the effect of plasmons is created, in microwave bands. The average cell size of both structures is equal to $p \ll \lambda_g$ and therefore satisfy the condition for effective homogeneity. To achieve a negative ϵ behavior from a thin wire structure the excitation electric field E has to be parallel to the axis of wires so as to induce a current along them. This generates equivalent dipole moments with plasmonic type permittivity as a function of frequency and expressed as,

$$\epsilon_r(\omega) = 1 - \frac{{\omega_{pe}}^2}{\omega^2 + j\omega\zeta} \tag{3.2}$$

where,

$$\omega_{pe} = \sqrt{2\pi c^2/[p^2 ln(p/a)]} \tag{3.3}$$

c is the speed of light, a represents the radius of the wires and ω_{pe} is the electric

plasma frequency, tunable in the GHz range, while

$$\zeta = \epsilon_0 \frac{(p\omega_{pe}/a)}{\pi\sigma} \tag{3.4}$$

where σ is the conductivity of the metal. The frequency dependency of the permittivity can be expressed as

$$\epsilon_r < 0, \quad \text{for } \omega < \omega_{pe} \tag{3.5}$$

For this material permeability is $\mu = \mu_0$, since no magnetic materials is present. The assumption made in the analysis is that the wires are much longer than wavelength, which implies the excitation is far below the first resonance. The other type of material shown in Fig. 3.3 is the split-ring resonator (SRR) structure. If the magnetic field H is perpendicular to the plane of the rings, resonating currents are induced in the loop and these generate magnetic dipole moments. The plasmonic-type permeability frequency is of the form

$$\mu_r = 1 - \frac{F}{\omega^2 - {\omega_{0m}}^2 + j\omega\zeta} \tag{3.6}$$

where, $F = \pi(\frac{a}{p})^2$ with a being the inner radius of the smaller ring and magnetic resonance frequency tunable at GHz is given by

$$\omega_{0m} = c\sqrt{\frac{3p}{\pi ln(2wa^3/\delta)}} \tag{3.7}$$

w is the width of the rings, δ radial spacing between the rings and $\zeta = 2pR'/a\mu_0$ with R': metal resistance per unit length.

$$\mu_r < 0, \quad \omega_{0m} < \omega < \frac{\omega_{0m}}{1-F} \tag{3.8}$$

where $\omega_{pm} = \frac{\omega_{0m}}{\sqrt{1-F}}$ is the magnetic plasma frequency. The difference between ϵ of thin wires structures and μ of SRRs is that the thin wire is a non-resonant structure

and the SRR is a resonant one. To put this discovery in context and looking at the history of metamaterials in general it is found that some of the interesting research had been done on complex media such as metamaterials, though not known by the same name. The next paragraph continues the discussion of the same.

Complex media has been investigated by various scientists since late 19th century and most part of 20th century. Artifical materials have been studied for much longer period. In 1898, Sir J.C.Bose conducted experiments on chiral media using twisted structures. Similarly, early twentieth century saw Lindman, who used helices embedded in host media to study chirality. In 1948, Kock modified the refractive index of artificial media [18]. The 1940s saw an extensive research on periodic structures. It is worth noting here from [19], in 1941 Mandelshatam noticed that for given two media Snell's law mathematically allows two solutions for a given angle of incidence θ_i, the possible angles of refraction can be θ_r or $\pi - \theta_r$. He also presented physical structures with negative phase velocity. Malyuzhinets in 1951 presented a transmission line model of Composite Left Hand Right Hand propagation. It is also speculated that the first paper on hypothetical medium with DNG constitutive parameters might have been presented by Sivukhin in 1957. He had noted that such a media with DNG parameters would be backward media. Silin discussed "negative refraction" in context of periodic structures in 1959. Variants of SRR can be found in 1952 textbook authored by Schelkunoff and Frris. 1980s and 1990s comprehensive studies on chiral and bi-isotropic media were conducted.

The periodic structures which are also used in use today and having the similar conceptual background as metamaterials can be traced back to 1940s, Brillouin conducted studies on wave propagation in periodic structures and described them in terms of negative space harmonics of the Fourier series. Pierce and colleagues investigated the backward amplification in traveling wave tubes. From these studies it backward waves are known to be a result of higher order modes. They are

associated with periodic structures with a period of half wavelength or multiple of half wavelength. Also, the conventional backward wave structures are dominated by diffraction/scattering and cannot be characterized in terms of ϵ or μ. Therefore, the use of the term "structures" on contrary to "materials".

MTMs operate in fundamental mode in which guide wavelength is much less than the unit cell dimensions. In such a case constitutive parameters are well defined. To get an insight, the comparison between real materials and MTMs is paramount. The real materials available in nature are generally made of molecules. These molecules are separated by Angstroms act as unit cells which induce electrical behavior expressed as permittivity of the material. In MTMs the distance between the unit cell is of the order of centimeters. For example, microwave bands L-X electrical size of the unit cell reduces to $p \ll \frac{\lambda}{10}$. Maxwell's equations is used to arrive at a general model to represent LH waves below. We know that

$$\begin{aligned} \nabla \times \vec{\mathcal{H}} &= \frac{\partial \vec{\mathcal{D}}}{\partial t} + \vec{\mathcal{J}}_{\mathcal{E}}, && \text{(Faraday's Law)} \\ \nabla \times \vec{\mathcal{E}} &= -\frac{\partial \vec{\mathcal{B}}}{\partial t} - \vec{\mathcal{J}}_{\mathcal{M}}, && \text{(Ampère's Law)} \\ \nabla \cdot \vec{\mathcal{B}} &= \rho_{\mathcal{M}}, && \text{(Solenoid Law)} \\ \nabla \cdot \vec{\mathcal{D}} &= \rho_{\mathcal{E}}. && \text{(Gauss's Law)} \end{aligned} \tag{3.9}$$

where, $\vec{\mathcal{E}}$ (V/m) and $\vec{\mathcal{H}}$ (A/m) represent electric field and magnetic field intensity, $\vec{\mathcal{D}}$ (C/m^2) and $\vec{\mathcal{B}}$ (W/m^2), electric flux density and magnetic flux density, J_E (A/m^2) and J_M (V/m^2) is the electric current density and magnetic current density and $\rho_{\mathcal{E}}$ (C/m^3) and $\rho_{\mathcal{M}}$ (C/m^3) represent electric charge and magnetic charge densities respectively. In addition, if the medium is linear and non-disperive(ϵ, μ do not depend on ω). The frequency domain condition known as the entropy condition must be satisfied by LH constitutive parameters. LH media are necessarily dispersive, however for this derivation we consider weak dispersion and proceed to arrive at the constitutive

relations shown below.

$$\vec{\mathcal{D}} = \epsilon_0(1+\chi_e)\vec{\mathcal{E}} = \epsilon_0\epsilon_r\vec{\mathcal{E}} \tag{3.10}$$

$$\vec{\mathcal{B}} = \mu_0(1+\chi_m)\vec{\mathcal{H}} = \mu_0\mu_r\vec{\mathcal{H}} \tag{3.11}$$

χ_e and χ_m are the electric and magnetic susceptibilities and $\epsilon = 8.854 \times 10^{-12}$ (F/m) and $\mu_0 = 4\pi \times 10^{-7}$ are the permittivity and permeability of free space respectively, ϵ_r and μ_r represent the relative permittivity and permeability of the material and can be expressed as

$$\epsilon_r = \epsilon' - j\epsilon'' = \epsilon'(1 - j\tan\delta_e) \tag{3.12}$$

$$\mu_r = \mu' - j\mu'' = \mu'(1 - j\tan\delta_m) \tag{3.13}$$

The imaginary parts of ϵ and μ in the above equations account for losses due to dielectric damping and finite conductivity. Similarly, magnetic damping and finite magnetic conductivity make up the losses for μ. For a generic phasor with time dependence

$$\vec{\mathcal{Y}}(\vec{r},t) = Re[\vec{\mathcal{Y}}(\vec{r})exp^{+j\omega t}] \tag{3.14}$$

where, $\vec{\mathcal{Y}}$ represents the phasor form of any physical quantities in Maxwell's equation, unlike (3.9) which is the time domain representation, and the constitutive relations written as

$$\begin{aligned}
\nabla \times \vec{H} &= \frac{\partial \vec{D}}{\partial t} + \vec{J_E}, && \text{(Faraday's Law)} \\
\nabla \times \vec{E} &= -\frac{\partial \vec{B}}{\partial t} - \vec{J_M}, && \text{(Ampère's Law)} \\
\nabla \cdot \vec{B} &= \rho_M, && \text{(Solenoid Law)} \\
\nabla \cdot \vec{D} &= \rho_E. && \text{(Gauss's Law)}
\end{aligned} \tag{3.15}$$

and

$$\vec{D} = \epsilon\vec{E} \tag{3.16}$$

$$\vec{B} = \mu\vec{H} \tag{3.17}$$

Let us consider a plane wave,

$$\vec{E} = \vec{E_0}\exp^{-j\vec{k}.\vec{r}} \tag{3.18}$$

$$\vec{H} = \frac{\vec{E_0}}{\eta}\exp^{-j\vec{k}.\vec{r}} \tag{3.19}$$

where, $\eta = \frac{|\vec{E}|}{|\vec{H}|}$ is the wave impedance. Let us consider a lossless medium ($\epsilon'' = \mu'' = 0$) for simplicity in regions without sources ($J_E = J_M = 0$). For an RH medium

$$\nabla \times \vec{E} \quad = \quad -j\omega\mu\vec{H} \tag{3.20}$$

for the given plane wave [29], we have

$$\begin{aligned}
\nabla \times [\Psi\vec{A}] &= \Psi\nabla \times \vec{A} + \nabla\Psi \times \vec{A}, \\
\nabla \times \vec{E} &= \exp^{-j\vec{k}.\vec{r}}\nabla \times \vec{E_0} + \nabla(\exp^{-j\vec{k}.\vec{r}}) \times \vec{E_0}, \\
\nabla(\exp^{-j\vec{k}.\vec{r}}) &= \exp^{-j\vec{k}.\vec{r}}\nabla(-j\vec{k}.\vec{r}), \\
\nabla(exp^{-j\vec{k}.\vec{r}}) &= -j\vec{k}exp^{-j\vec{k}.\vec{r}}, \\
\nabla \times \vec{E} &= -j\vec{k}\exp^{-j\vec{k}.\vec{r}} \times \vec{E_0}.
\end{aligned} \tag{3.21}$$

$$\nabla \times \vec{E} = -j\vec{k} \times \vec{E} \tag{3.22}$$

$$-j\vec{k} \times \vec{E} = -j\omega\mu\vec{H} \tag{3.23}$$

Therefore,

$$\vec{k} \times \vec{E} = \omega\mu\vec{H}, \tag{3.24}$$

Similarly, it can be shown that

$$\vec{k} \times \vec{H} = -\omega\epsilon\vec{E}, \tag{3.25}$$

Equations (3.16) and (3.17) form the right handed triad. For a LH medium with $\epsilon, \mu < 0$ the relationship between propagation constant $\vec{k}$ and the fields and material parameters can be expressed as

$$\vec{k} \times \vec{E} = -\omega|\mu|\vec{H} \tag{3.26}$$

$$\vec{k} \times \vec{H} = +\omega|\epsilon|\vec{E} \tag{3.27}$$

The phase velocity v_p given by

$$v_p = \frac{\omega}{k}\hat{k} \tag{3.28}$$

where, $\hat{k}$ is the unit vector along the direction of $\vec{k}$. In a LH medium phase velocity is in opposite direction compared to that in a RH medium. All the derivation assumes TEM propagation in a homogeneous and isotropic medium and the wave number 'k' can also be written as

$$k_n = n\frac{\omega}{c} \tag{3.29}$$

where,

$$n = \pm\sqrt{\epsilon_r\mu_r} \tag{3.30}$$

In a LH medium k < 0 leads to n < 0 such that $|n| = -n$. Therefore, it can be concluded that the index of refraction is negative in a medium with double negative parameters.

3.3 Split Ring Resonators

Split-ring resonators are concentric metal rings consisting of split in between. The first of its kind was proposed by Pendry consisting of two concentric rings sepa-

rated by a gap between inner and outer rings. The split-ring resonators are resonant structures on contrary to other types of metamaterials which are non-resonant periodic structures. From an antenna perspective, they resemble a capacitively loaded loop antenna. When operated slightly above resonant frequency the local scattered magnetic field and the incident field are out of phase resulting in negative magnetic polarization. Different geometries for split ring resonators are available and shown in Fig. 3.4 and other structures such as broadside coupled SRR and non-bianisotropic SRR are also found in literature which are generally used in situations where cross polarization is not desirable. A single split-ring resonator is shown in Fig. 3.5. The magnetic behavior of this structure is found to be enhanced due to the presence of the split in the ring. At resonance most of the energy gets stored in the tiny gap between the rings. This concentration of electromagnetic energy in a small volume results in an enormously enhanced energy density resulting in nonlinear magnetic behavior of the structure.

Fig. 3.6 shows a lumped circuit model for a single split ring. It acts as a RLC resonator with resonant frequency $\omega_0 = \frac{1}{\sqrt{LC}}$. The radius of the ring and width 'w' affect the resonant behavior of the structure and eventually effect the permeability it exhibits and remain important design parameters. From a design standpoint having a thinner ring would result in higher inductance and a larger gap would mean increase capacitance of the structure. The slits are wider than the thickness of the substrate on which the rings are fabricated. When a external time varying magnetic field at angular frequency ω is applied perpendicular to this structure an electromotive force is generated in SRRs. Considering the electrical size to be small a quasi-static behavior is expected and this can be used as model in the design of these rings. The current lines take an almost circular path with displacement current lines existing in the split. The whole device hence behaves as an LC resonator driven by an external electromotive force.

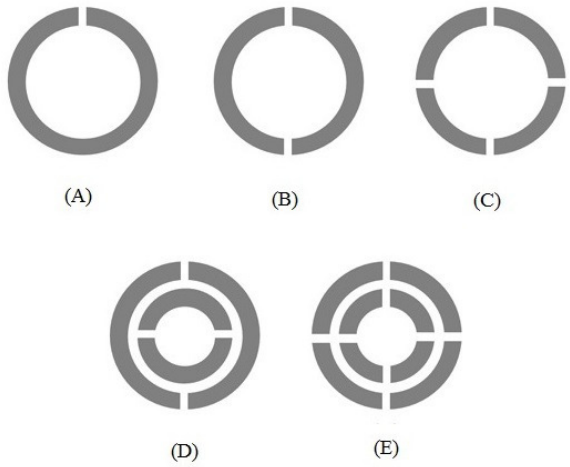

Figure 3.4: Different topologies available for the design of split-ring resonators

Fig. 3.4 shows different topologies of split ring resonator. The structures can have more than one split in the rings and also consist of multiple rings. Conventional SRRs with single split can be operated upto few terahertz (THz). But for frequencies upwards of 100 THz single split ring resonators are chosen as it is easy to fabricate these structures. The other reason for the choice is that they are resonant for different polarizations and propagation directions. Furthermore, other structures such as two cut and four cut structures seen in Fig. 3.4 (B)–(E) have similar behavior however the rate of increase in resonance frequency is larger for SRR with multiple splits.

Comparing different topologies it is found that increase in the number of splits increases the magnetic resonance as overall capacitance of the system decreases drastically. Inserting a ring inside the SRR decreases magnetic resonance. For one cut and two cut resonator structures the amount of decrease of ω_m is found to be around 1 GHz. But four cut structures don't exhibit this behavior. It can be noted that the four cut structures are symmetrically oriented which reduces the mutual capacitances of the inner and the outer rings [30]. All these factors are taken into considerations in choosing the appropriated structure for this work. The resonant frequency for this

work is around 1.22 GHz and hence a one cut structure is preferred over others. In the next section we discuss EC-SRR which is SRR with a concentric ring inserted with splits on the ring are opposite with respect to each other.

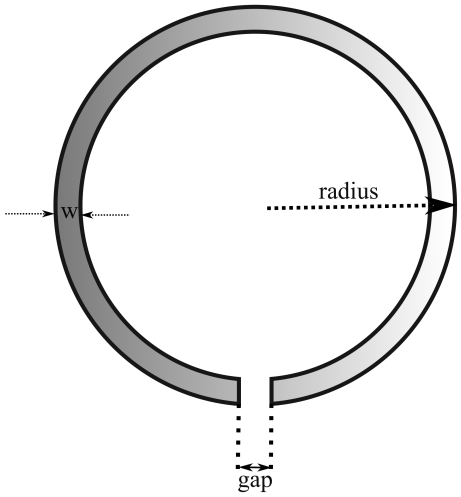

Figure 3.5: Single SRR with design varibles r1: radius of the ring, w: width of the rings

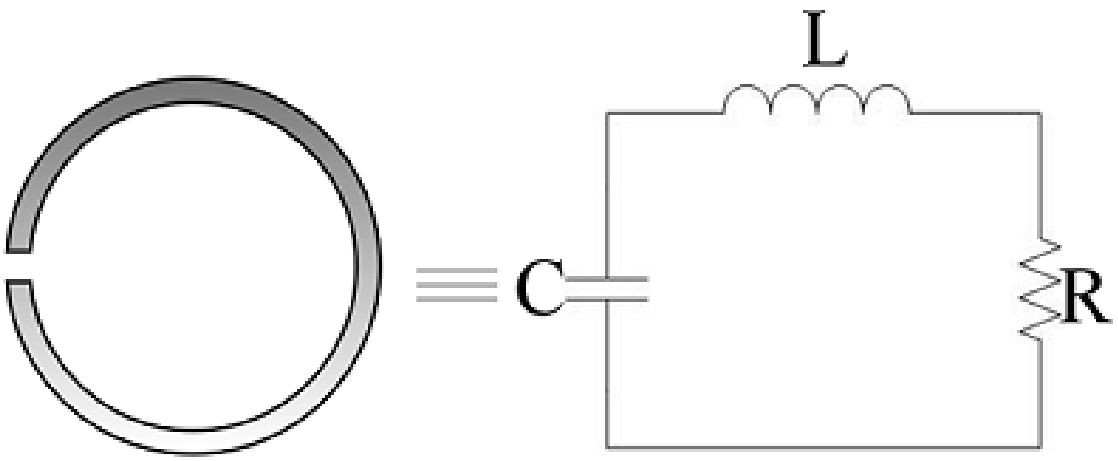

Figure 3.6: SRR represented as lumped circuit elements with split modeled as capacitor and metallic modeled as a combination of series inductance and capacitance.

3.4 Edge Coupled Split Ring Resonator

A concentric split-ring resonator known as edge coupled split ring resonator consists of two concentric split rings as shown in Fig. 3.7. The additional ring in EC-SRR geometry adds a degree of freedom to the design. The presence of which also provides stronger coupling compared to the single SRR. The distance between the rings d, width of the ring w and the split in the ring s control the electromagnetic behavior of the structure.

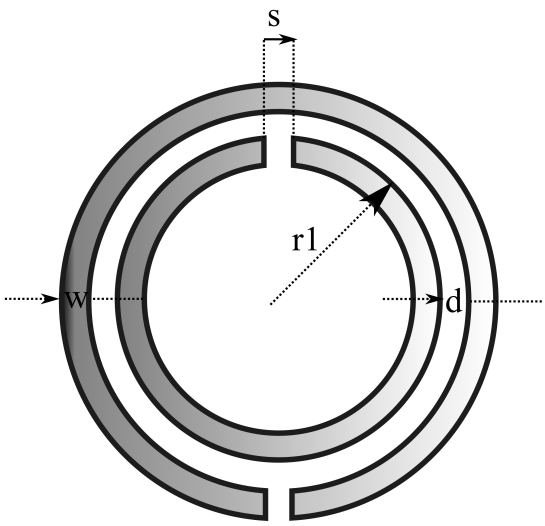

Figure 3.7: A complementary SRR of radius:r1, distance 'd' between the rings and width 'w' these design variables affect the permeability of the structure.

The circuit model for EC-SRR accounts for mutual inductance and coupling capacitance between two concentric rings as shown in Fig. 3.8. On application of a magnetic field perpendicular to the structure the whole device behaves a LC circuit driven by external electromotive force. The proper excitation of the structure requires a time-varying magnetic field with a significant component in the axial direction. Complementary split ring resonators (CSRR) and SRR exhibit cross polarization. This means they can be excited either magnetically or electrically. This is the cause of bi-anisotropic behavior of the rings. At this point it is also important to think

about the polarizations of the wave exciting the rings. This leads to the inclusion of parasitic structures which can interact with the existing electric field not parallel to them would in turn affect the overall resonant frequency of the structure.

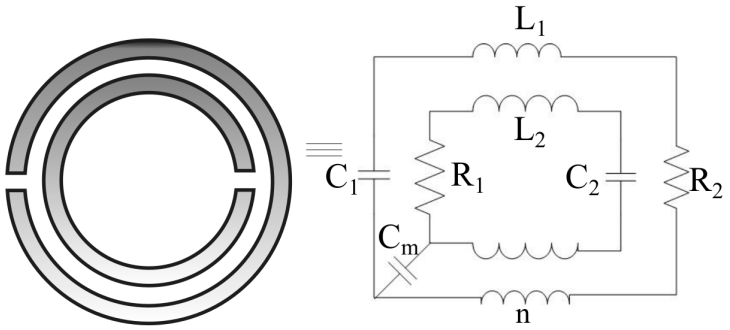

Figure 3.8: Equivalent lumped circuit model of EC-SRR consisting of an additional mutual capacitance between the rings modeled as C_m and mutual inductance.

This work capitalizes on the MNG behavior EC-SRR which is preferred over SRR as it provides stronger coupling with the field. The EC-SRRs are ease to fabricate and can be printed on a dielectric material. This makes the structures planar and robust and ease in integration with other components. An array of EC-SRRs behave as a negative μ material. Finally, this property can be used in altering the boundary condition of a wave and used in combination with DPS materials to achieve interesting phenomena. The one this work is interested in is the modification of radiation properties of the antenna which is presented in detail in the next chapter.

CHAPTER 4: BOW TIE ANTENNA WITH METAMATERIALS

The theory discussed in earlier chapters is used in the design, fabrication and measurement of the proposed antenna consisting of a bow tie antenna with edge coupled split ring resonator (EC-SRR) and a modified topology of EC-SRR in the H-plane of the antenna. The antenna is designed to operate from 1.15 GHz– 1.4 GHz with a center frequency at 1.22 GHz. The metamaterials to be designed has a plasma frequency above 1.2 GHz so that it behaves as MNG within the functional bandwidth of the antenna. The design involves loading metamtaerial structures in such a way that magnetic field of the antenna interacts with the metamaterials resulting in the change of far field directive property of the antenna. Design process of antenna, proposed metamaterial in EC-SRR and modified EC-SRR are discussed separately with a goal of answering the specific questions relevant to the design.

4.1 Proposed Antenna Design

An antenna configuration of bow tie antenna with metamaterials is proposed to achieve selective directivity. Bow tie antenna has an omnidirectional radiation pattern. The proposed antenna configuration aims to alter the radiation pattern in the H-plane of the antenna. From the theory found in literature it is shown that metamaterials used with antennas can lead to optimization of antenna performance. The solution to alter directivity relies on the use a mu negative material (MNG) to achieve increased directivity in E-plane of the antenna relative to the H-plane. Since the H-plane of the antenna consists of magnetic field components it is useful to think in terms of magnetic materials and MNG materials in particular so as to utilize the field component to excite meta-resonators such as SRRs. EC-SRR is preferred for its

simplicity and compatibility it offers to this design. The resonant frequency of the EC-SRR is given by

$$\omega_r = \frac{1}{\sqrt{LC}} \tag{4.1}$$

where L and C are the capacitance and inductance due to the geometry of the structure. The presence of metamaterial with resonant frequency lying the bandwidth of operation of antenna is helpful for this purpose. The capacitance and inductance in the equation shown above are found to be the functions of width, gap and radius of the structure described in section 3.4. These structures resonate when excited by a magnetic field perpendicular to the plane of the dielectric hosting them. The substrate used is FR-4 with a dielectric constant of 4.4. In the context of waves, the wavenumber k

$$k = \omega\sqrt{\mu_r \epsilon_r} \tag{4.2}$$

for a MNG medium μ is negative the negative valued permeability has a narrow band above resonance of the material resulting in the inhibition of signal propagation in the direction of the medium. EC-SRR used with the antenna are intended to produce this effect. A modified EC-SRR consisting of metal posts is also used to demonstrate the shifting the band of operation. This is due the addition of capacitive coupling resulting from the interaction of electric field components and metal posts used to create the media. This is useful in shifting the operational bandwidth and resonance with selective directive.

The anisotropy of the material poses constraint on the orientation of the metamaterial around the antenna,for a negative permeability metamaterial like EC-SRR. The rings can be cross polarized with electric and magnetic field. In this work, magnetic polarization is preferred so as create a medium with effective negative permeability in the near field of the antenna. The variation in polarization and angle of incidence lead to variation in the material property. They are characterized by uniaxial permittivity

tensors as shown

$$[\mu] = \begin{bmatrix} \mu_{xx} & 0 & 0 \\ 0 & \mu_{yy} & 0 \\ 0 & 0 & \mu_{zz} \end{bmatrix} \tag{4.3}$$

Unlike, simple isotropic medium the material properties of metamaterials are expressed in terms of permittivity and permeability tensors. It is important to take note of the anisotropic nature of the materials especially when it is integrated with source of excitation in this case bow tie antenna. ECSRR is is an ideal metaresonator for this purpose. The design and simulation are divided into two parts and presented in sections that follow: the first part addresses the design of antenna. The second part deals with the design and simulation of proposed metamaterials. A comparison is made and insights drawn are discussed in the end.

4.2 Design and Simulation of Bow Tie Antenna

Antenna is designed to operate in L-Band (1.12 GHz - 2 GHz). The band of frequencies are of interest because they are used in satellite communications and GPS applications. This band is chosen to demonstrate selective directivity which can be further extended to other applications especially next generation wireless communications operating at higher frequency. One of the advantages of selective directivity is it reduces interference and increases the efficiency of the system. The advantages of Bow tie antenna over other broadband dipole is that it can be fabricated on a substrate and structure is flexible enough to incorporate material on the substrate or around the antenna.The radiating elements are laid on a FR-4 with a relative permittivity of 4.4. The antenna is optimized to operate at a center frequency 1.22 GHz. The bandwidth characteristics of the antenna are in direct correlation with the angles made by the triangular radiating elements at the feed. The length of the antenna for this design is based on the studies [16, 31]. It is has been shown that the impedance bandwidth for a conical monopole starts at around $\frac{\lambda}{4}$ and extends up

to $\frac{\lambda}{2}$. As Bow Tie antenna is the finite and planar version of the bi-conical antenna and rules applicable to bi-conical antenna and bow tie remains the same however, the sensitivity of input impedances as the function of frequency need to taken into consideration. This constraint is due to truncation of bow tie antenna which would otherwise have be of infinite length. The radiation pattern and polarization remains unchanged in the bandwidth of operation. The antenna is linearly polarized hence ensuring the proper excitation of EC-SRR.

Resonance at 1.22 GHz is achieved when the length of the total length of the antenna is in between 61.5 mm to 123 mm. Each triangle is of length is equal to the half the difference between total antenna length minus the gap. The gap is generally in the range of 2 mm-7.5 mm. The arithmetic mean of the lowest and highest value in the range is used to arrive at 5 mm for the gap between two metallic conductors. A set of simulations involving parametric analysis is used to determine the exact length of the antenna. Unlike, thin wire dipoles limited in bandwidth because of thinner wires and high reactance beyond resonance, taper of the bow tie antenna can be visualized as a wire that increases in diameter this in turn provides room for current dispersion so as to exhibit frequency independent characteristics. In the case of bi-conical antennas input impedance remains unchanged for relatively large band compared to a common dipole antennas if the taper angle is large. The broadband characteristics is defined by nearly constant resistance and zero reactance in the band of interest. A bow tie antenna has broadband characteristics if the flare angle is in between $30° < \alpha < 90°$. Input impedance is found to decrease as the cone angle increases. The taper angle or flare angle $\alpha = 45°$ is found to be optimal for this design.

The next logical step is to determine the choice of the feed for the antenna. The antenna is feed using a coaxial cable. The reason for the choice of the feed is that half wave dipoles have an input impedance nearly equal to 70Ω at resonance. RG-59U

coaxial cable with characteristic impedance of 50Ω provides good match with lower reflections. It is also important to note that the feed mechanism may vary depending on the design, one can feed the antenna with a coplanar stripline or a microstrip feed with a quarter wave transformer to match the feeding/receiving end. The trade-off is, unlike coaxial cable, some part of the electromagnetic energy is confined to dielectric using a microstrip feed and existence of fringing effects results in unwanted coupling between the elements in the near field of the antenna, stripline feed on the other hand, suffer from losses and need higher quality dielectrics affects the bill of materials. Furthermore, mode of propagation in a microstrip for example is quasi-TEM. On the other hand, coaxial cable propagates TEM waves and is shielded so that the energy does not radiate outwards. The overall system has a near field component in split ring resonators making the choice of coxaial cables more feasible compared to others.

Ansys HFSS, full wave 3D electromagnetic solver, is used to create a 3D model of bow tie antenna consisting of two triangular elements on FR-4 of thickness 1.6 mm separated by gap of 5 mm and connected by coaxial cable is simulated. Coaxial cable is laid out on one of the radiating parts of the antenna. The inner conductor of the coaxial cable has a diameter equal to 0.81 mm, with outer conductor with a diameter of 5 mm. The two conductors are radially separated by a polystyrene The Fig. 4.1 shows the antenna in discussion. Analysis is set up with maximum number of passes equal to 30 and delta S equal to 0.01 satisfying either of the two conditions results in convergence. A frequency sweep from 1 GHz to 1.5 GHz is added as the part of the analysis. A wave port is assigned to the unconnected end of bow tie and a radiation boundary is provided to obtain far field reports. The polystyrene face is assigned the wave port on contrary to an integration line between the conductors. Initially, the total antenna length is set to 80 mm and based on the simulation results the antenna resonance is intended to be tuned to the frequency of interest. The flare angle is set

to 45° in the first set of simulations.

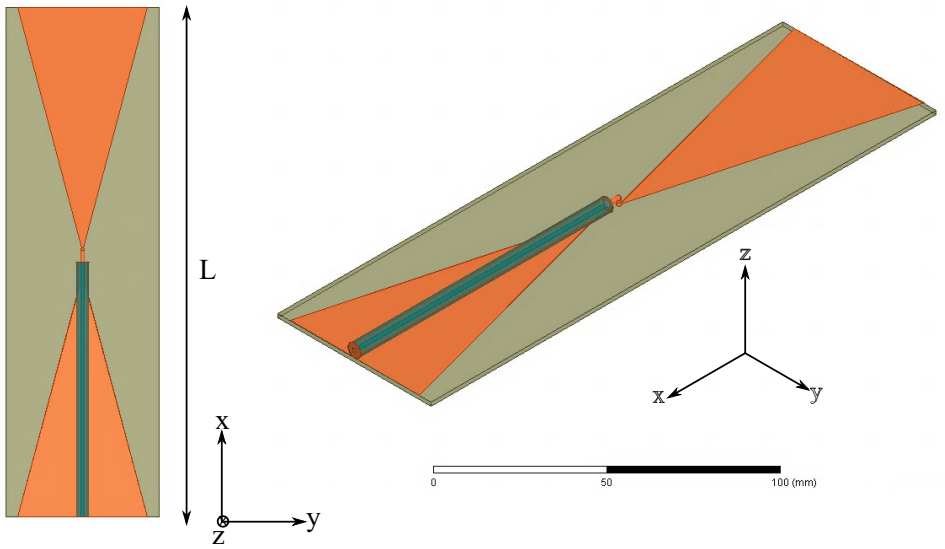

Figure 4.1: Top view of the antenna on the left and isometric view on the right.Radiating elements are placed on the substrate the variable total length of the antenna 'L' is the variable used in parametric sweep to arrive at design specifications in terms of center frequency and bandwidth.

Parametric analysis is set up to optimize the antenna to meet design specifications. The sweep resulted in the value for L= 78.65 mm, antenna center frequency equals 1.22 GHz. The bandwidth is based on return loss of the antenna, the region below -10dB on the S_{11} plot is reported as bandwidth. At this point, it is also found that better performance is achieved by increasing the surface area of the metal. So for the next simulation of the antenna additional triangular radiating elements are fabricated on either sides of the substrate and connected to each other using vias. The substrate thickness remains the same at 1.6 mm. The resulting antenna is found to have better performance. The antenna is shown in Fig. 4.2 has vias etched all the way from top to the bottom of the substrate connecting two metal triangles on either sides. More vias provide better connectivity and reduce losses associated with the substrate. Nearly eight vias are used for connection between the metal layers for each triangle of the bow tie. The metal thickness is 0.035 mm on either sides of the substrate.

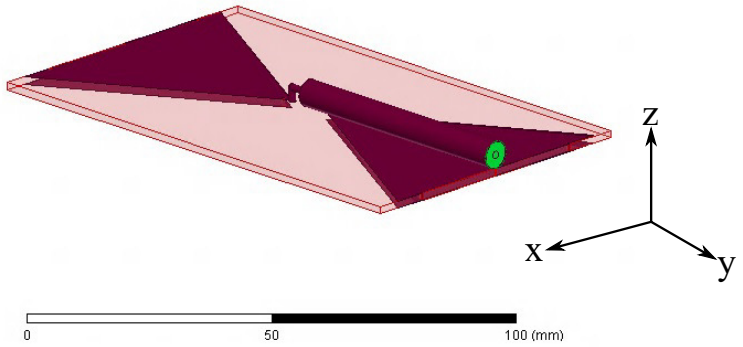

Figure 4.2: Diametric view of Bow Tie antenna with conducting elements on either side of the FR-4 substrate connected by vias.

The vias in the previous version of the antenna are further replaced by solid triangles etched inside the substrate. The motivation to change the design is to enable strong coupling to near field components. A periodic array of EC-SRR fill up the space around the antenna. Also, this model can be practically realized with an antenna with upwards of 10 vias used for the connection compared to the earlier version of the antenna using nearly 8 for connections in the earlier design. Fig. 4.3 shows the 3D model of the final antenna. The feed is integrated into one of the triangular element. This done to make space for metamaterials arrays and provide robustness to the structure. The other advantage this model provides is symmetry which is important to obtain same spacing between the top and bottom layers of the metamaterials. Since the feed is the part of the antenna it provides better match compared to being mounted on top of the antenna simulation and soldered in the final fabricated model. The metamaterials from a distance are approximated as a homogeneous isotropic media. The width of the substrate in the X-axis of the antenna is equal 40 mm. For simulations the coax is terminated as seen the Fig. 4.3 and assigned a waveport for excitation.

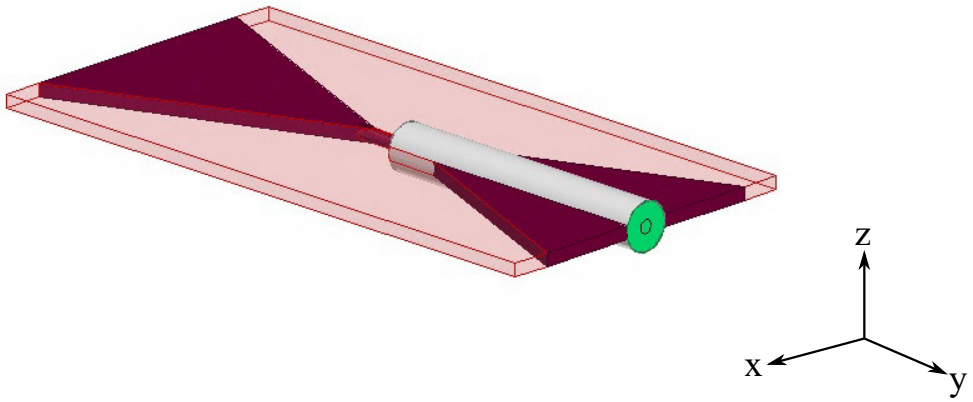

Figure 4.3: Bow tie antenna with coaxial feed as the part of the antenna, for simulations purposes radiating elements are modified to extended all the way through the FR-4 substrate of thickness 1.6 mm.

The input impedance, reflection co-efficient, directivity at different frequencies and 3D polar plots are used as metrics to validate the design specifications. The magnitude of real and imaginary parts of the input impedance of the antenna indicate the point of resonance and is the function of antenna length. The antenna length is varied to adjust zero crossing reactive part to the point where the real part is maximum. The design is verified for input impedance of the antenna, reflection co-efficient, directivity at the center frequency, directivity for a frequency with the band in this case it is chosen to be 1.32 GHz, 3D polar plot of the radiation pattern showing gain in linear scale in the far field. On yielding satisfactory results from the simulation the next part of the design process is undertaken. The simulation results of the antenna impedance is shown in Fig. 4.4. The real part of input impedance of bow tie antenna equals 56 Ω at 1.22 GHz where the reactance equals zero. The characteristic impedance of the coaxial feed is equal to 50 Ω. The antenna is found to be impedance matched with the feed hence eliminating the need for a matching network between the feed and the antenna.

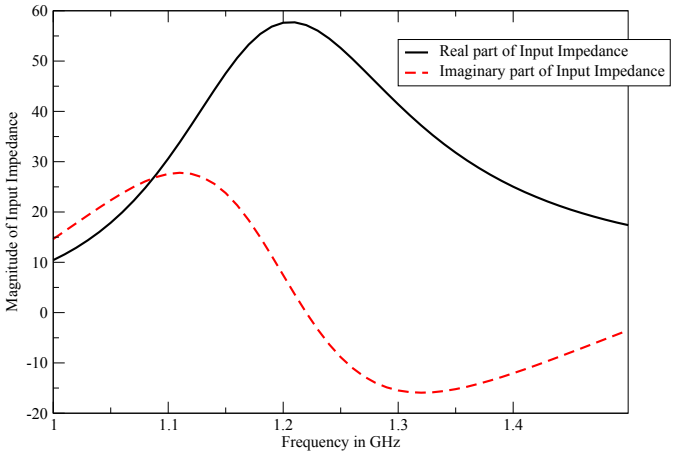

Figure 4.4: Magnitude of real and imaginary part of input impedance plotted over frequency.

The fractional bandwidth of the antenna is equal to 18.8 % the slope of reactance curve at the center frequecy is much smaller compared to off resonant frequencies. At resonance the total energy stored in the antenna switches between stored magnetic energy and electrical energy, effectively appearing to cancel reactance at the given frequency. The real part of the antenna has the peak value at resonance indicating maximum radiation. At frequency beyond resonant frequency the antenna reactance is dominated by capacitance of the structure and below the resonant frequency it is dominated by the inductance. This implies energy remains within the antenna without being radiated. This also emphasizes the need for losses to account for radiation. The real part of the impedance is equal to 56 Ω implying a good match between the 50 Ω source and the antenna. The impedance profile of the antenna remains fairly the same over the band. The antenna remains linearly polarized within the band. As discussed in the theory the variation in the gap and the length affect the imaginary part of the antenna shifting the zero crossing to a different frequency. Hence it can be seen that the choice of length and the gap are ideal for this antenna to reasonate at 1.22 GHz.

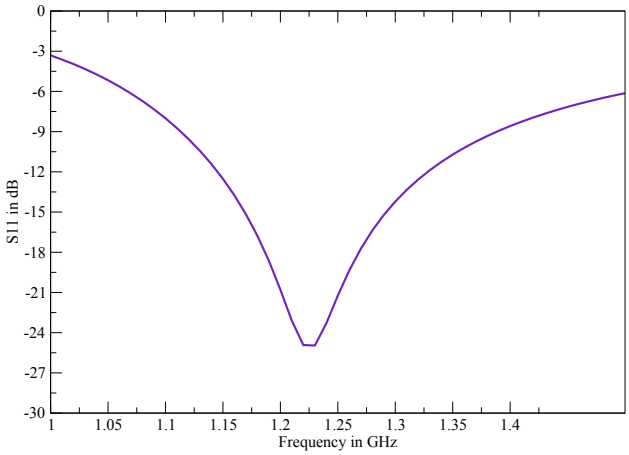

Figure 4.5: Input reflection co-efficient of the antenna as the function of frequency. The region of curve below -10dB is between 1.13 GHz- 1.36 GHz.

The input impedance profile and the reflection co-efficient indicate the operational bandwidth of the antenna to be 230 MHz. In addition to this, the far field parameters such as directivity and 3D radiation patterns are also determined. In order to simulate for the far field the radiation boundary around the antenna must be at a distance in between $\lambda/4$-$\lambda/2$, at the lowest frequency of interest, apart. In this case lowest frequency is 1 GHz. Mesh operations must be applied on the box with length equal $\lambda/6$ of the of the highest frequency of interest which is equal to 1.5 GHz. Meshes play an important role in ensuring the accuracy of computation. It is desirable to have higher resolution in the regions where the fields of interest exist. Hence the mesh assignment for measuring the radiated fields of the antenna. An infinite sphere is set up with default ranges for ϕ and θ to capture far field radiation. The rectangular plot of the antenna directivity at 1.22 GHz and 1.32 GHz is shown in Fig. 4.6 and Fig. 4.7 respectively. Both plots represent the directivity of the antenna in the plane defined at $\phi = 0$. The other plane would be at $\phi = 90°$ not presented here. Table 4.3 summarizes important results obtained from the simulation of the antenna.

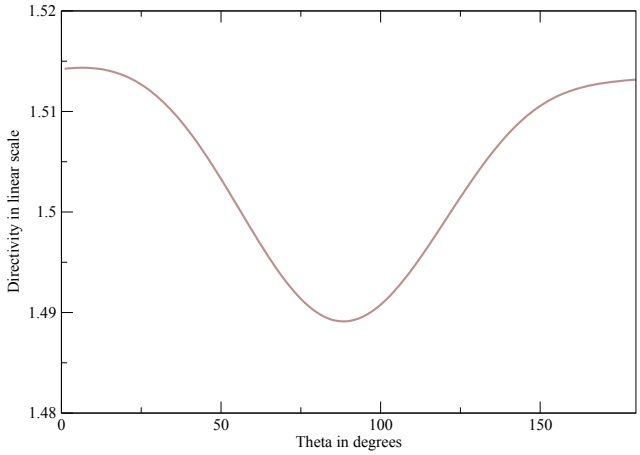

Figure 4.6: Directivity of the antenna at 1.22 GHz in linear scale as the function of θ in degrees at $\phi = 0$. The directivity is relatively low equal to 1.49 in E-Plane of the antenna.

The directivity of the antenna is nearly the same around the antenna. In the plane parallel to antenna (Y-axis) the value is 1.514 in linear scale compared to 1.492 in the plane perpendicular to the antenna (Z-axis).

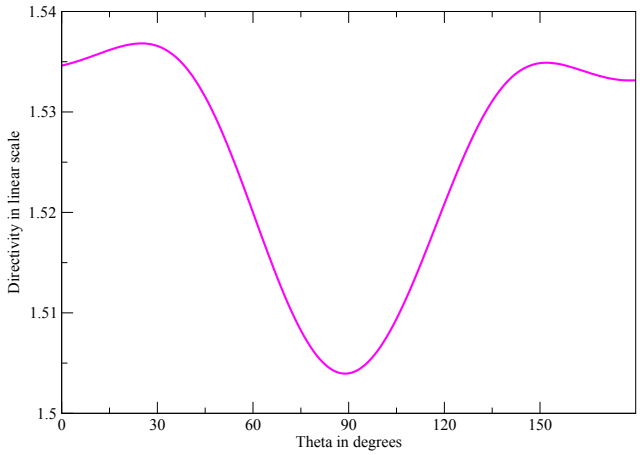

Figure 4.7: Directivity of the antenna at 1.32 GHz in linear scale as the function of θ in degrees at $\phi = 0$. The directivity is equal to 1.505

Directivity at 1.32 GHz is shown in Fig. 4.7. This frequency is chosen since it is 100 MHz from the resonant frequency which is a reasonable value for the shift in resonance in the presence of a material with negative permeability. Also, it is found from the simulations that the antenna configuration with modified EC-SRR is resonant around this frequency which makes it suitable frequency for comparison.

Finally, the 3D polar plot radiation pattern of the antenna as a function of θ and ϕ is observed in the Fig. 4.8. The gain of the antenna in linear scale at 1.22 GHz is equal to 1.537 and 1.514 at 1.32 GHz. The radiation pattern is broadside omni-directional with no radiation in the Y-axis. The antenna simulation results are found to be consistent with design specifications.

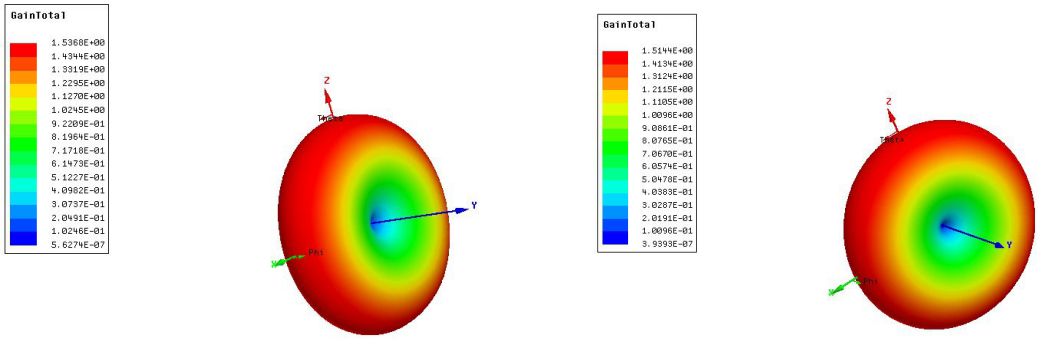

(A) (B)

Figure 4.8: (A) 3D polar plot of antenna gain at 1.22 GHz (B) Antenna gain at 1.32 GHz

The results found from this part of the simulation is tabulated in Table 4.3. The antenna with 18.8 % qualifies as broadband antenna. The input impedance is close to the input impedance of RG-59 hence the antenna has better has less reflections at the feed point. The gain of the antenna is reasonable for a conventional broadband antenna.

Table 4.1: The table summarizes the important results obtained from the simulation of the antenna.

Antenna Parameters	Value
Center Frequency	1.22 GHz
Fractional Bandwidth	18.8 %
Input impedance at 1.22 GHz	56 Ω
Directivity at 1.22 GHz in the E-plane	1.49

4.3 Design and simulation of proposed Metamaterial

The next step in is the design a edge couple split ring resonator (EC-SRR) to resonate at 1.2 GHz. This frequency range is chosen in particular because it is close to 1.22 GHz the resonant frequency of the antenna and is one of two frequencies utilized by GPS known as L2. The design variables that determine the frequency of operation depend on the radius of the outer ring(r_1), split in the ring(s) and the separation between the inner and outer rings(d). From Pendry's seminal work, it is known that electric field parallel to thin wire yields negative ϵ and split ring resonators combined with metal posts exhibit double negative behavior as shown by Smith and colleagues, the novel model is a variation of CSRR presented in these works. The EC-SRR are modified to include a metal post perpendicular to the electric field to provide an additional degree of freedom, the interaction of the field and the metal in the given polarization is used to tune the capacitance of the split ring resonators. This leads to the shift in frequency response of the overall configuration. Unlike, conventional SRR the proposed EC-SRR provide a capacitive loading of the antenna. The design of the rings remains the same. However, the metal post has the dimension effect the overall capacitance of the structure. Here the width of the metal post is same as the split between the rings. Fig.4.9 shows the modified CSRR and Table 4.2

lists the dimensions for this design.

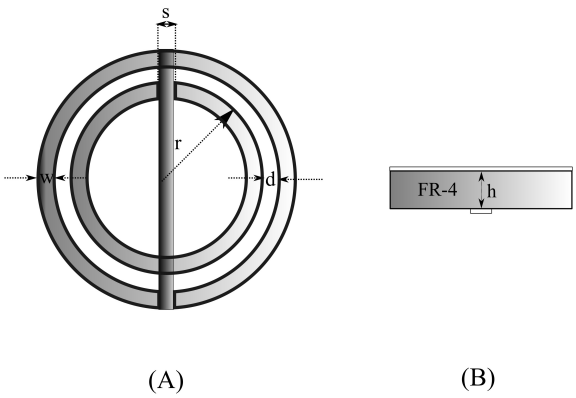

Figure 4.9: Modified CSRR with metal post on the other side of the substrate.(A) Top view of the modified CSRR (B)Side view of the modified SRR where the post and CSRR are separated by substrate thickness. For FR-4 substrate used in this design equal h=1.6 mm.

The dimension of the CSRR are calculated using theory presented in Chapter 3 and tabulated in Table 4.2.

Table 4.2: The table summarizes the dimension of a single unit cell of EC-SRR.

Design Variables	Value
r1	8.6 mm
d	0.4 mm
w	1.2 mm
s	0.75 mm
a	20 mm

A 3D model based on the design is generated using HFSS and simulated. In order to confirm the negative permeability of the proposed metamaterial structure a parameter extraction algorithm is used. The parameter extraction method by Zsabò

and team at

4.3.1 Parameter Extraction Procedure

In electromagnetics, a material is characterized by its wave impedance, electric permittivity, magnetic permeability and refractive index. It is important to determine these parameters in order to predict the electromagnetic behavior of the material. For a material ϵ_r and μ_r determine the electromagnetic behavior and other parameters can be derived from them. Hence to verify the electromagnetic behavior of the proposed structure we need to extract ϵ_r and μ_r and verity negative μ of the proposed metamaterials in particular. There are various algorithms used for parameter extraction. The material parameter extraction algorithm based on Kramer-Kronig relationship developed by Zsolt Zsabò et. al. is used in this work. The algorithm uses S-parameters to determine wave impedance and the imaginary part of the refractive index.

The metamaterial structures are place inside a parallel plate waveguide with side wall assigned magnetic boundary and top and bottom assigned electric boundary as shown in the Fig. 4.10. The remaining sides of the rectangle are assigned as wave ports that are de-embedded by the distance between the excitation and object inside the waveguide. This sets the reference plane of the wave at the metamaterial. The electric field is parallel to X-axis and the magnetic field to the Z-axis as illustrated in Fig. 4.10. This set up inclusive of metamaterial forms a two port structure. Transmission and Reflection co-efficients of the structure are obtained from simulations. The steps of the algorithm are as follows: S_{11} and S_{12} are used to determine the wave impedance and refractive index for a plane wave with normal incidence on the metamaterial. The parallel plate wave guide ensures the excitation of the metamaterial with a plane wave. The relation between S_{11} and S_{12} with wave impedance and refractive index is given by

$$S_{11} = \frac{R_{01}(1 - \exp^{j2N_{eff}k_0d_{eff}})}{1 - {R_{01}}^2 \exp^{j2N_{eff}k_0d_{eff}}} \tag{4.4}$$

$$S_{21} = \frac{(1 - {R_{01}}^2)\exp^{j2N_{eff}k_0d_{eff}}}{1 - {R_{01}}^2\exp^{j2N_{eff}k_0d_{eff}}} \tag{4.5}$$

R_{01} is the function of complex wave impedance given by

$$R_{01} = \frac{(Z_{eff} - 1)}{(Z_{eff} + 1)} \tag{4.6}$$

N_{eff} is the complex refractive index represented as $N_{eff} = n_{eff} + j\kappa_{eff}(\omega)$, where n_{eff} is the refractive index, k_0 is the free space wave number and ω is the angular frequency. The complex wave impedance Z_{eff} can be written in terms of S-parameters using the previous relations as

$$Z_{eff} = \pm\sqrt{\frac{(1 + S_{11})^2 - S_{21}^2}{(1 - S_{11})^2 - S_{21}^2}} \tag{4.7}$$

Also,

$$\exp^{jN_{eff}k_0d_{eff}} = \frac{S_{21}}{1 - S_{11}R_{01}} \tag{4.8}$$

Complex refractive index is given by

$$N_{eff} = \underbrace{\frac{Im[ln(\exp^{jN_{eff}k_0d_{eff}})] + 2m\pi}{k_0d_{eff}}}_{n_{eff}} + j\underbrace{\frac{-Re[ln(\exp^{jN_{eff}k_0d_{eff}})]}{k_0d_{eff}}}_{\kappa_{eff}} \tag{4.9}$$

m in the equation denotes an integer known as branch index, Applying the Kramer-Kronig relationship to the above equation following the steps for simplification in [32] results in

$$N_{eff} = \sqrt{\epsilon_{eff}\mu_{eff}} \tag{4.10}$$

and,

$$Z_{eff} = \sqrt{\frac{\mu_{eff}}{\epsilon_{eff}}} \tag{4.11}$$

The units of Z_{eff} is in Ohms. The effective magnetic permeability and electric permittivity are calculated as

$$\mu_{eff} = N_{eff} Z_{eff} \tag{4.12}$$

$$\epsilon_{eff} = \frac{N_{eff}}{Z_{eff}} \tag{4.13}$$

The mathematical equations derived are formulated into an algorithm implemented using MATLAB code returning the μ_{eff} and ϵ_{eff} values for the given dimension. The thickness of the slab d_{eff} appearing in the equations is the length of the unit cell. For multiple unit cells effective thickness is the sum of the lengths of all the unit cells.

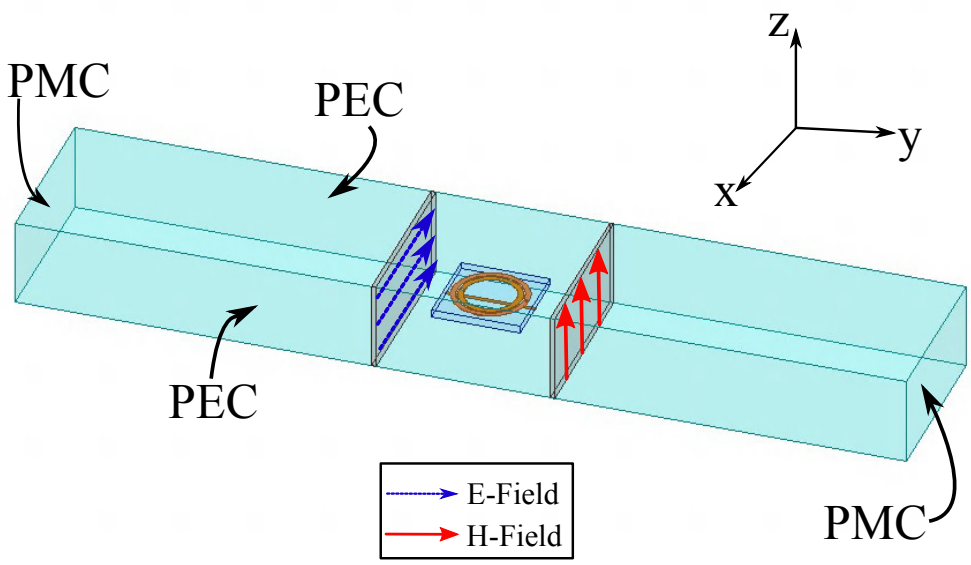

Figure 4.10: Modified CSRR with metal post place inside a parallel plate waveguide with top and bottom plates assigned PMC boundary and the direction of magnetic field is shown as dotted red line.

The MATLAB code is provided with the following input, returning the effective permittivity, permeability and refractive index of the MUT(Material Under Test) as the output of the code. The input file consists of:

1. Frequency in GHz : Kramer-Kronig integral uses S-parameters obtained over large frequency range. Hence enough number of frequency samples must be provided.

2. Magnitude of S_{11}
3. Phase of S_{11} in Radians
4. Magnitude of S_{12}
5. Phase of S_{12} in Radians
6. Effective length of the unit cell in meters

The assignment of appropriate boundary conditions for plane wave incidence followed by the extraction routine is used in the design process of EC-SRR and modified EC-SRR. The parameter extraction confirms the behavior of the designed unit cell as a negative Mu material. The results from the extraction and for the dimension listed in Table 4.2 are shown in Fig. 4.11 and Fig. 4.12.

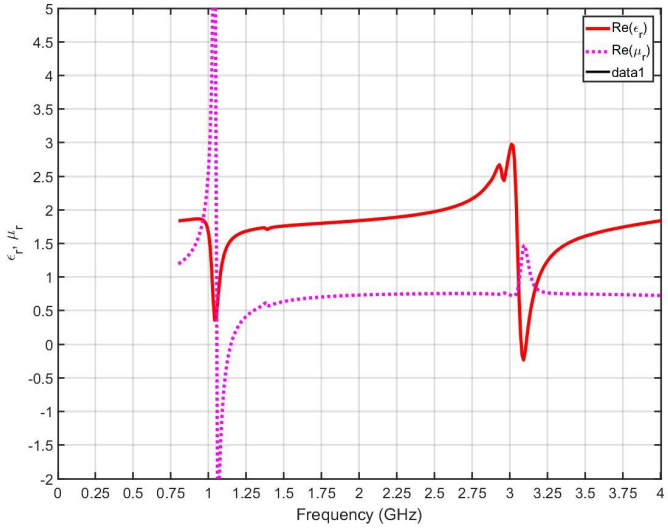

Figure 4.11: Real and Imaginary parts of electric permittivity and magnetic permeability.At 1.2 GHz μ_r is negative and ϵ_r of the MUT is positive.

The different possible refractive index results from the solution to the branching problem with 'm' branches described in the paper. It can be observed that one the value of permeability is negative and a positive refraction is also possible for this value. For this work DNG is not a requirement hence NRI is not stressed upon.

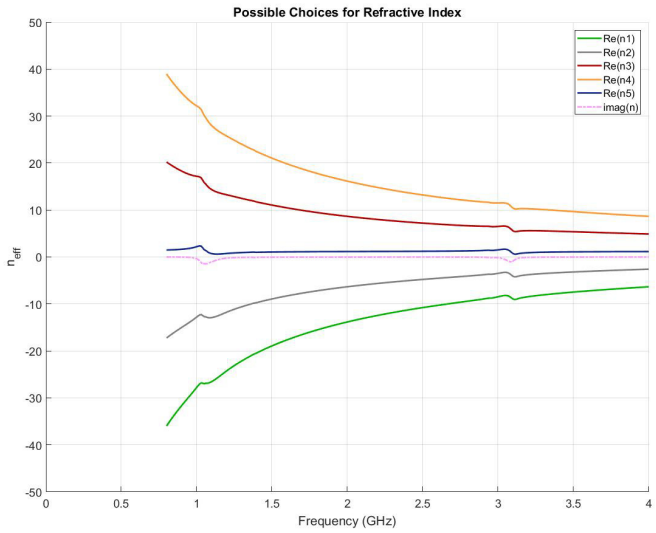

Figure 4.12: Possible values of refractive index.

A 4x5 array of modified EC-SRR shown in Fig. 4.13 is designed with the gap in the substrate containing the array to include antenna in between.

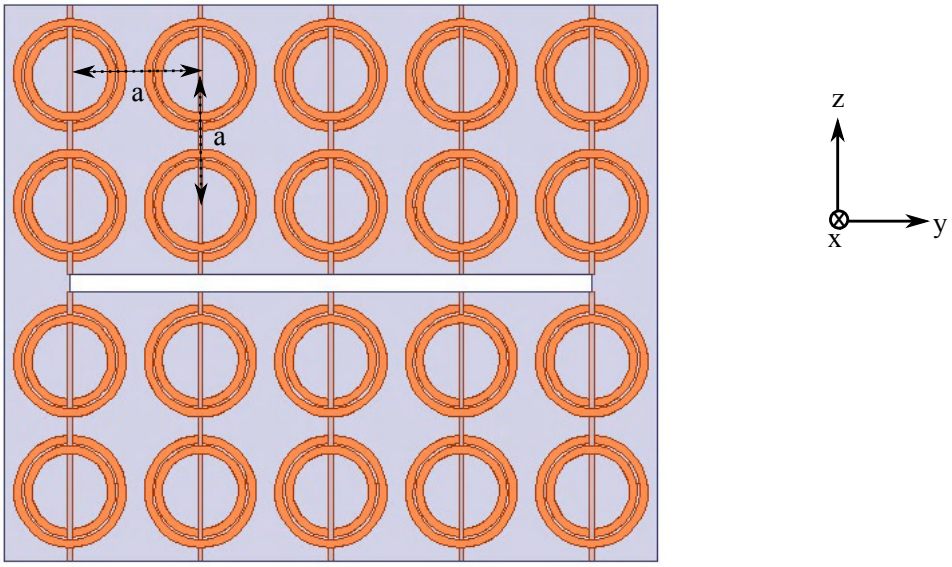

Figure 4.13: 4x5 modified EC-SRR array with metal posts. Each unit cell size 'a' is equal to 20 mm and the width of the metal post is 0.4 mm

To start with the antenna is simulated with three such arrays mounted symmetrically from the center of the antenna. The simulated results showed that increase in

the number of arrays lead to better performance as as it increases the thickness of the effective medium around the antenna. Five such arrays are mounted on the antenna as illustrated in Fig. 4.14

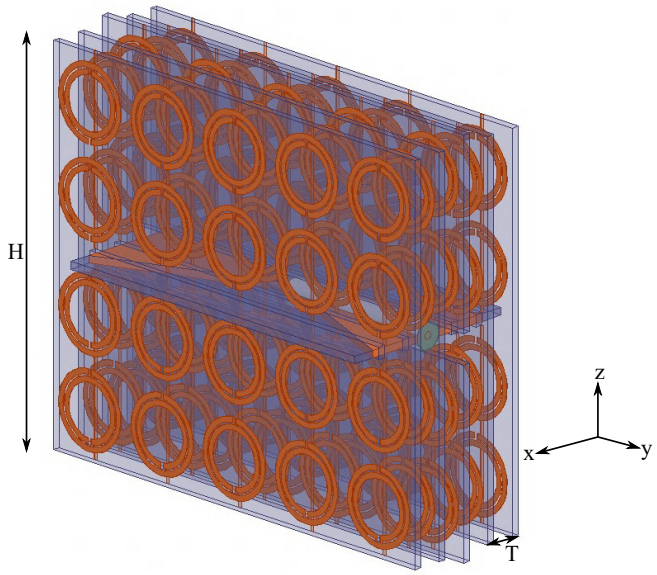

Figure 4.14: Five 4x5 arrays of modified EC-SRR is placed on top and bottom of the antenna. The height of the metamaterial is H = 82 mm and the distance between the arrays is T = 6.75 mm Each unit cell size 'a' is equal to 20 mm and the width of the metal post is 0.4 mm

Similarly, five structures with 4x5 array consisting of conventional EC-SRR without metal posts as unit cell form the basis for second simulation using metamaterial and is shown in Fig.4.15. The dimensions and design of the elements remain the same this makes it easier to compare and single out the effect of metal post on the performance of the antenna. The dimensions of the radiation box is changed according to the dimensions for the total structure. The new dimension finds the addition of H to the length of the box in Z-axis compared to the earlier version for only the antenna. The two antennas are simulated using HFSS and compared with each other. The orientation of the split rings is important in both cases due to the dependency of polarization of the wave on the resulting properties of the material. To achieve negative permeability the split on the larger ring must be oriented in the

direction as seen in Fig.4.14 and Fig. 4.15. It can also be observed that the substrate of the array is very close to the antenna itself but it does not touch the antenna as in the case using metal posts this may lead to a short and deviation in behavior.

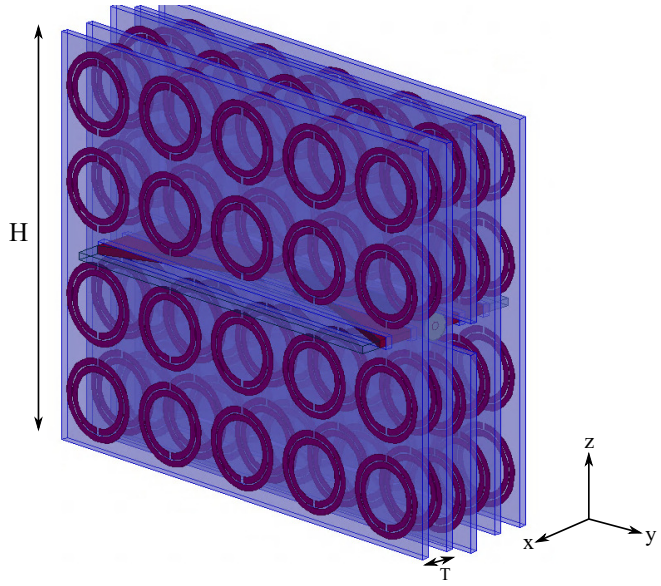

Figure 4.15: Five 4x5 arrays of modified EC-SRR array is placed on top and bottom of the antenna. The height of the metamaterial is H = 82 *mm* and the distance between the arrays is T = 6.75 *mm* Each unit cell size 'a' is equal to 20 *mm* and the width of the metal post is 0.4 *mm*

HFSS simulation results and antenna measurement results are presented and discussed in the next section.

4.4 Results and Discussion

The antenna and metamaterials are fabricated on a 1/16" FR-4 substrate using LPKF prototyping machine. The reflection co-efficient of the antenna configuration is measured using Aniritsu Shockline Vector Network Analyzer. The far field radiation pattern is measured outdoor using an over the air set up. This section summarizes the results from simulation and measurements. The results are presented in the following order: input impedance, reflection co-efficient, directivity and 3D radiation patterns of antennas with metamaterials and compared with antenna without metamaterials. This is followed by comparison of simulated and measured results.

4.4.1 Simulation Results

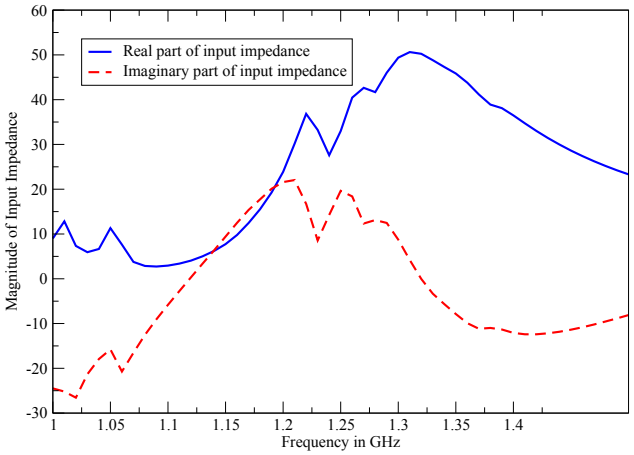

Figure 4.16: The real and imaginary parts of input impedance are displayed in the figure with dotted line representing the imaginary part

The input impedance profile of the antenna is same as the bow tie, however the resonance is shifted to 1.32 GHz. The modified EC-SRR in the near field itself being a resonant structure perturbs the resonance of the antenna. This interaction is primarily due to the magnetic polarization giving rise to currents in the structure which result in fields that interact with the near fields of the antenna. This shift is useful as it provides scope with respect to tunning the antenna resonance using external materials. By engineering the appropriate micro-structures the resonance of the overall configuration can be adjusted to have desired value of resonance. It can also be observed that the characteristics of the antenna are no longer dependent on the antenna characteristics but the material around them. It is also important to note the change in boundary condition around the antenna. The wave impedance around the antenna is different than it would have been for free space. The antenna impedance at resonance at 1.32 GHz is equal to 50.24 Ω. This indicates a near perfect match between the source and the antenna.

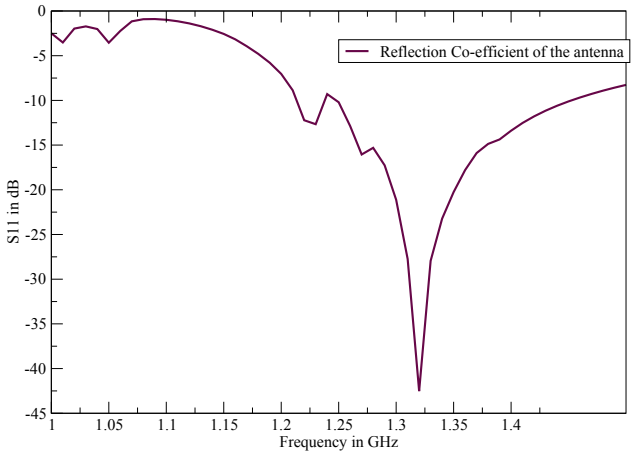

Figure 4.17: Reflection co-efficient of the antenna with modified EC-SRR in dB

The reflection co-efficient confirms better performance at 1.32 GHz as described earlier due to the match at the input. The -10dB bandwidth is 230 GHz. There appears to be a bump within the band of operation this is due to the non-linearity resulting from introduction from the elements in the near field of the antenna. The unit cell elements of the metamaterials themselves have magnetic performance due to the non-linearity introduced due to the discontinuities in the structure. Mathematically, the Lorentzian form of the curve confirms this behavior.

The directivity of the antenna observed at 1.22 GHz is shown in Fig. 4.18 it can be seen that the directivity is increased by two times in the E-plane of the antenna compared to the H-plane. The value of directivity is equal to 1.64 dB at $\theta = 90°$ and there is a 3.33 dB increase in directivity in plane defined by earlier value of θ compared to $\theta = 0°$. The simulations show an increased directivity which is the desired outcome to go ahead with the prototyping of the antenna model. However, the antenna itself resonates at 1.32 GHz on contrary to 1.22 GHz this is due to the presence of parasitic capacitances. The directivity of the antenna at this frequency is shown in the Fig. 4.19 as a function of angular variation in θ for a constant ϕ.

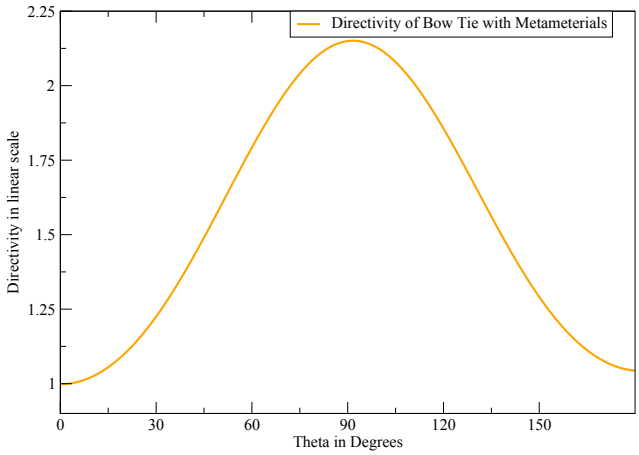

Figure 4.18: Directivity of the antenna operating at 1.22 GHz in linear scale for $\phi = 0$. The directivity is in the E-plane of the antenna is increased by a factor of 2.

The directivity of the antenna is again increased by a factor of two. The value of directivity at $\theta = 90°$ is equal to 2.13 on contrary to 1.06 in linear scale at $\theta = 0°$. In terms of dB the directivity of the antenna is 3.5dB more in the E-plane of the antenna compared to the H-plane.

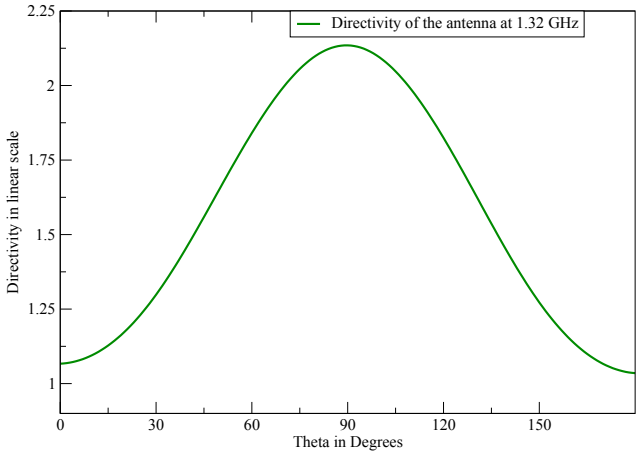

Figure 4.19: The rectangular plot of directivity of antenna with modified EC-SRR in linear scale at 1.32 GHz for $\phi = 0$.

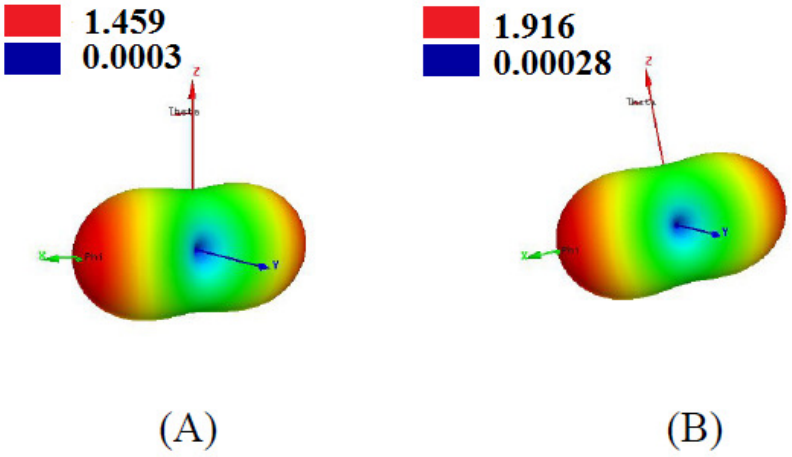

Figure 4.20: (A) Gain of the antenna with modified EC-SRR at 1.22 GHz (B) Gain of the antenna at 1.32 GHz in linear scale.

It can be seen in Fig. 4.25 that the radiation pattern of the antenna is not omnidirectional. It takes the form a directional radiation pattern with a grating lobe on the other side. the gain of the antenna at 1.22 GHz is 1.46 and 1.92 at 1.32 GHz which happens to be the point of resonance. The next set of curves present the simulation results for the antenna with conventional EC-SRR.

The input impedance plot in Fig. 4.21 reveals that the resonance of the antenna occurs at 1.28 GHz. The magnitude of real part of input impedance at frequency of resonance is equal to 60.73 Ω which is higher compared to the input impedance of the antenna with modified EC-SRR and antenna without any metamaterials. Fig. 4.22 shows the return loss of the antenna configuration two important observations that can be made are first, the bandwidth is larger than the other antenna configurations discussed so far and equal to 245 MHz and the frequency shift is less pronounced in comparison with modified EC-SRR. This is because there is no cross polarization effects that can alter the performance of the antenna in the absence of the metal posts keeping the orientation intact.

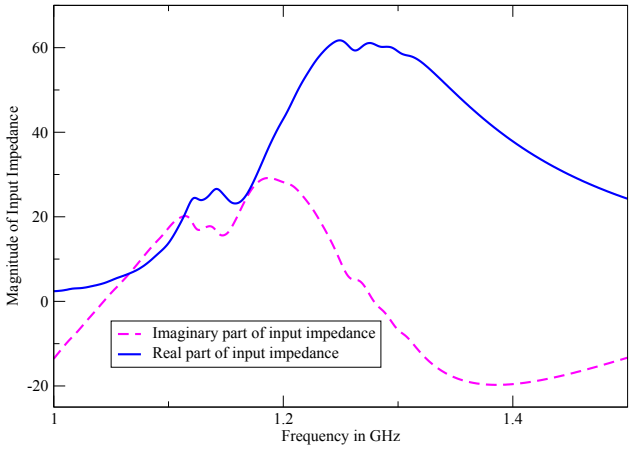

Figure 4.21: Real and imaginary part of the input impedance of the antenna with EC-SRR

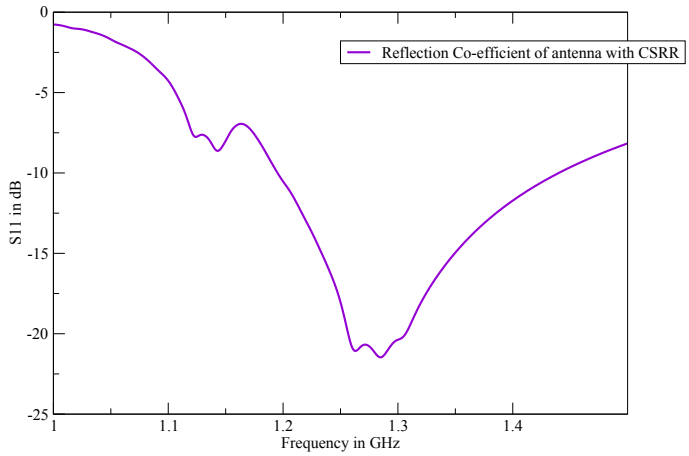

Figure 4.22: Reflection co-efficient of the antenna with EC-SRR

The -10dB bandwidth spans from 1.195 GHz to 1.44 GHz. The bandwidth remains nearly the same as it was for the antenna without loading. The directivity of the antenna in the E-plane at 1.28 GHz is again nearly twice compared with the directivity of the antenna in the H-plane.

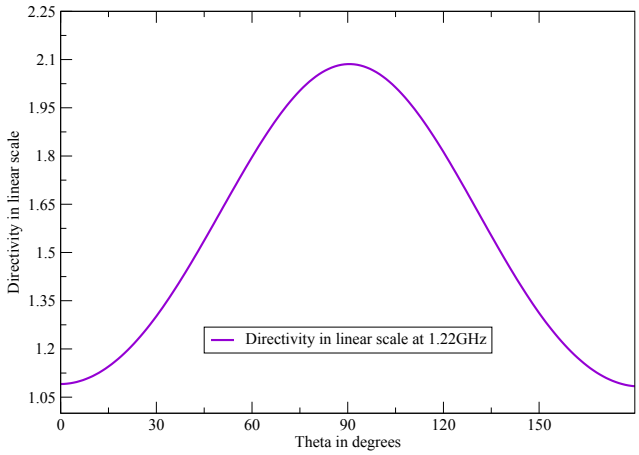

Figure 4.23: Directivity of the antenna with EC-SRR in linear scale at 1.22 GHz

Even though the antenna is resonant at 1.28 GHz, for comparison the directivity at 1.22 GHz and 1.32 GHz is reported. Fig. 4.23 and Fig. 4.24 shows the plot of directivity at these frequencies and directivity at $\theta = 90°$ is larger than at $\theta = 0°$. The results obtained here are consistent with the theory and goals this work aimed to achieve in terms of directivity.

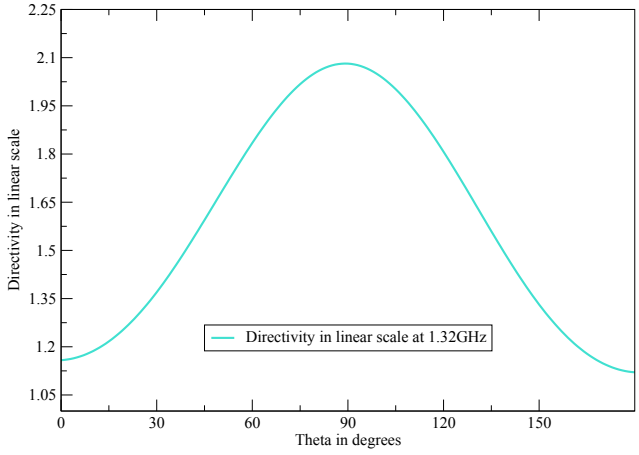

Figure 4.24: Directivity of the antenna in linear scale at 1.32 GHz

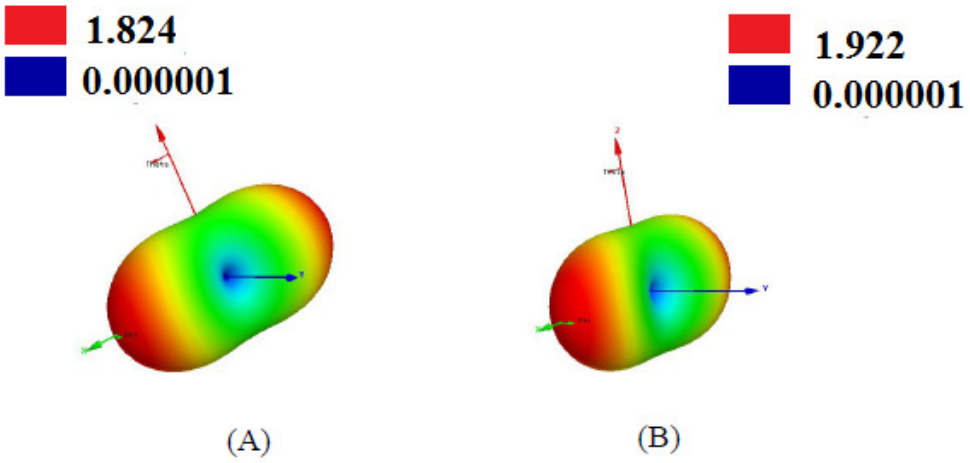

Figure 4.25: (A) Radiation pattern in terms of gain in linear scale of the antenna with EC-SRR at 1.22 GHz (B) Radiation pattern in terms of gain in linear scale of the antenna with EC-SRR at 1.32 GHz

The gain of the antenna is relatively higher compared to other configurations. The gain at 1.22 GHz is equal to 1.824 and at 1.32 GHz is equal to 1.922 respectively. The gain of the antenna at 1.32 GHz with metamaterials is much larger than the gain of the antenna without metamaterials. The gain for antenna with EC-SRR and with modified EC-SRR is almost the same at 1.32 GHz.

A radiation pattern is the plot of gain as a function of direction. Fig. 4.26 shows the 2D radiation pattern at $\phi = 0$ of the different antenna configurations. The gain of the antenna with EC-SRR is maximum at 1.22 GHz is larger than all other configurations. The gain of the antenna with modified EC-SRR is the lowest because the resonance of the antenna is shifted towards 1.32 GHz. For a the antenna configuration with modified EC-SRR the gain increases in the -10dB band. The plane of reference is $\phi = 0$ plane which represents the E-plane of the antenna. In figure shown the value of the gain for antenna without metamaterials, with EC-SRR and antenna with modified EC-SRR are 1.45, 1.48 and 1.82 respectively. The directivity of different antenna configurations is compared at 1.22 GHz and shown in Fig. 4.27.

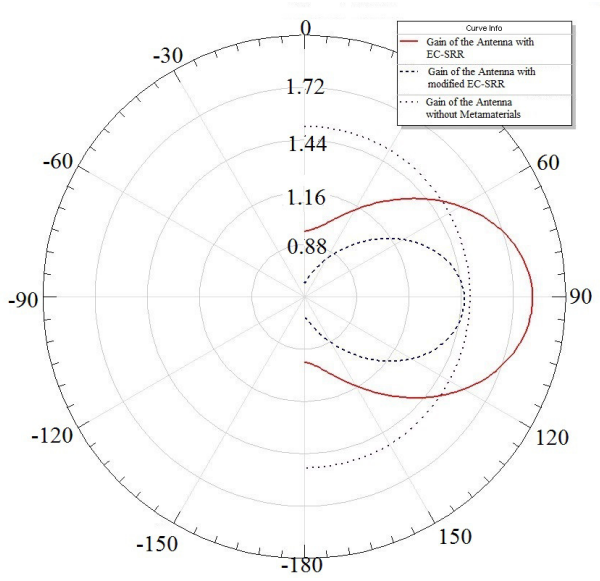

Figure 4.26: 2D radiation pattern at 1.22 GHz in the E-plane of the antenna with $\phi = 0$.

It is clearly observable that the directivity of antennas with metamaterials is significantly improved in the E-plane and the H-plane is reduced. In terms of directivity at 1.22 GHz the antenna with modified EC-SRR is greater than the antenna with EC-SRR. It is helpful to note that the electrical performance of the antenna is to be interpreted in terms of both gain and directivity.

Directivity only concerns with the ability of the antenna to receive signal in the particular direction rejecting the interfering signals in the other directions. The gain of the antenna, in a receiving configuration, describes how well the RF power received in a particular direction is converted into electrical power. It is found that the antenna performance in terms of both directivity and gain is enhanced for the antenna loaded with metamaterials in comparison to the antenna without loading. But one has to take note of the frequency shift in this regard. The Fig. 4.27 takes into account only one frequency. This comparison shows that the frequency response of the antenna is shifted in case of antenna loaded with metamaterials with post on contrary to the antenna with conventional CSRRs.

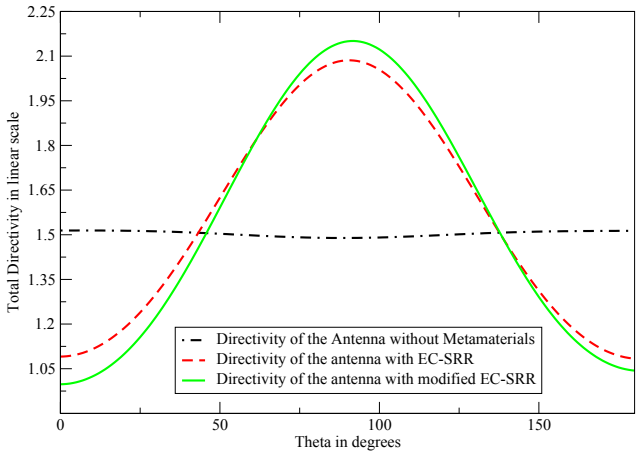

Figure 4.27: Directivity of different antenna configurations in linear scale at $\phi = 0$ and function of θ

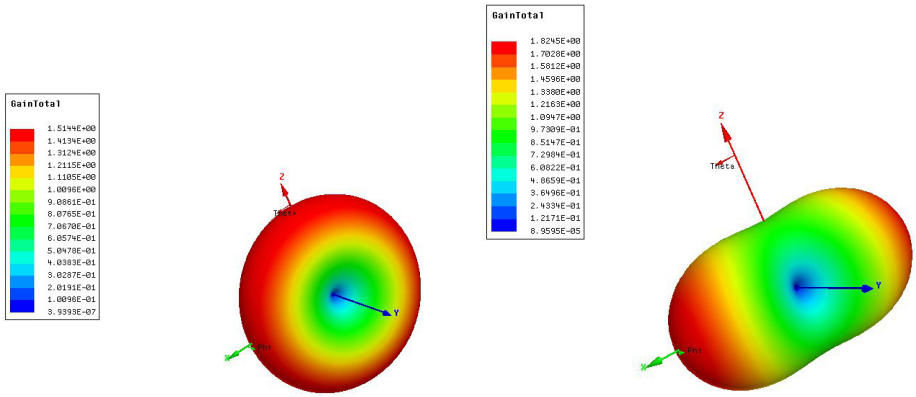

(A) (B)

Figure 4.28: .Radiation pattern of the antenna configurations representing gain total at 1.22 GHz (A) Omnidirectional radiation pattern of bow tie antenna (B) Directional radiation pattern of bow tie antenna with EC-SRR.

The plots of 3D radiation pattern with gain expressed in linear scale confirm directional propagation of the antenna. The gain of the bow tie antenna at 1.22 GHz is equal to 1.80 dB. The antenna configurations with metamaterials i,e., antenna with

EC-SRR at 1.28 GHz is 2.56 dB and for antenna with modified EC-SRR the gain of the antenna at 1.32 GHz is equal to 2.82 dB respectively. The polarization of all the configurations is found to be linear in the operating band.

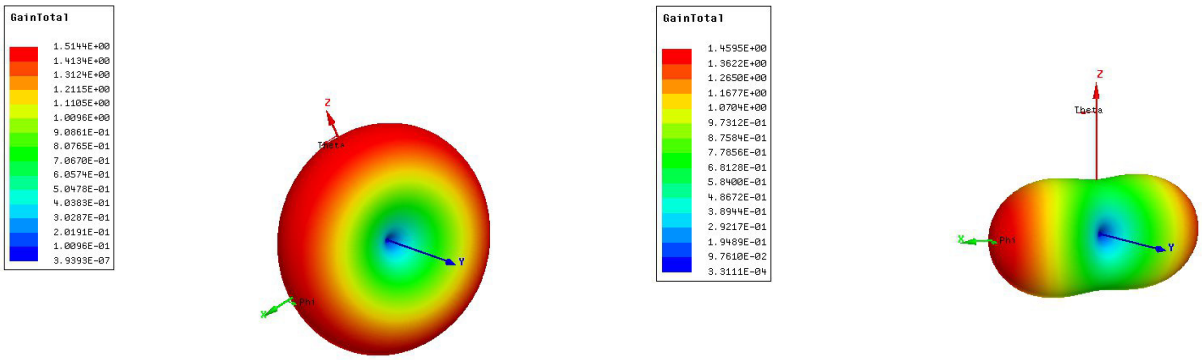

(A) (B)

Figure 4.29: Radiation pattern of the antenna configurations representing gain at 1.22 GHz.(A) Omnidirectional radiation pattern of bow tie antenna (B) Bow tie antenna with modified EC-SRR.

4.4.2 Measured Results

The fabricated antenna reflection co-efficients are measured and the resonance is found to be at 1.27 GHz and has a -10 dB bandwidth from 1.18 GHz to 1.41 GHz. The antenna is mounted with modified EC-SRR structure and the results obtained are plotted in comparison with simulated results of the antenna configuration. The -10 dB band along the frequency is found to be shift to the right of the graph. The feed of the antenna is soldered to the antenna and mismatch at these points would result in the degradation of the signal. Also, fabrication tolerances, especially in case of edge coupled split ring resonators would have led to the deviation from the ideal output. The losses in FR-4 is another major reason that can be attributed to the obtained results as the $\tan\delta$ of FR-4 is equal to 0.01 making it more lossy compared to other higher quality dielectrics. However, FR-4 serves as a more economical option

requiring extra care during fabrication and design. The surface waves in the dielectric are not accounted for in the simulations due to the use of solid metal in between the substrate as the antenna this assumption would affect the performance of the fabricated antenna. The mismatch in the connectors used with the antenna would also be responsible for the deviation observed. The resonance of the antenna itself occurs at 1.45 GHz and the -10 dB band is between 1.4 GHz- 1.55 GHz.

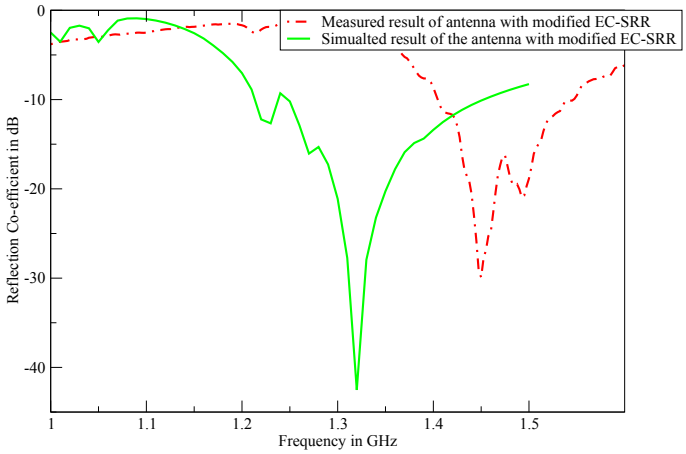

Figure 4.30: Simulated and measured reflection co-efficient of the antenna with modified EC-SRR.

For far field measurements of the antenna are performed outdoor. The feed horn is used for transmission and the bow tie antenna is operated in receiving mode oriented for H-plane measurements. The H-plane of the antenna is parallel for the first set of measurements. The antenna in turn is mounted on a setup which can be rotated to change the orientation of the antenna. The antenna measurements are taken for angular values ranging from 0 to 180°. The step size of each measurement is equal to 10°. A Keysight spectrum analyzer is connected to the antenna to determine the received power in dBm. The values are converted to linear scale using the relation

$$dBm = 10log\Big(\frac{P_{out}}{1mW}\Big) \tag{4.14}$$

where P_{out} represents power gain of the antenna. The values are divided by the maximum value of the power gain to obtain normalized results. The values are tabulated result is used to obtain the plot of normalized gain as a function of angular rotation of the H-plane is given as shown in Fig. 4.31.

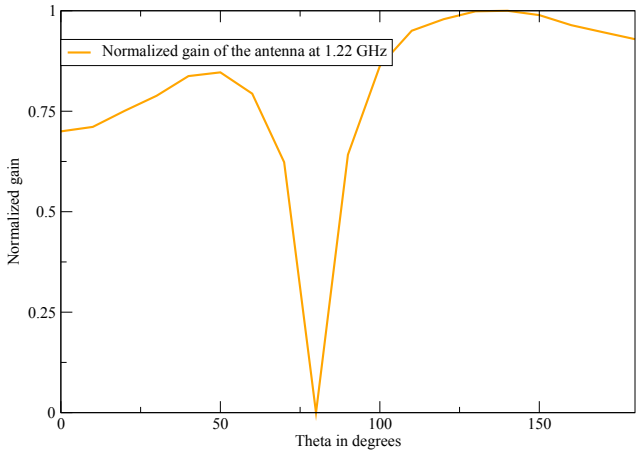

Figure 4.31: Measured radiation pattern in the H-plane of the antenna without metmaterials at 1.22 GHz

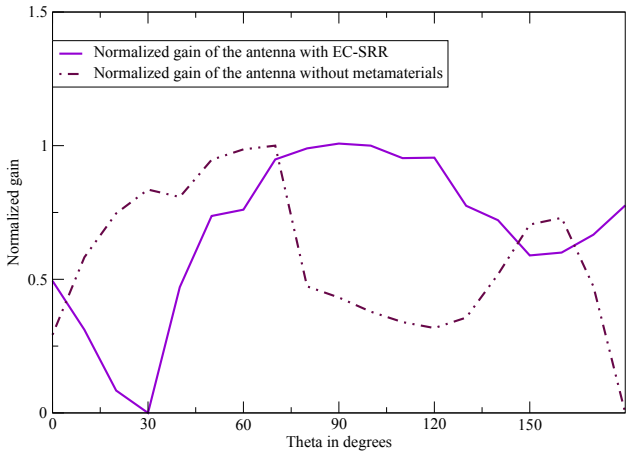

Figure 4.32: Measured radiation pattern in the E-plane of the antenna with and without metamterials at 1.45 GHz.

In the next set up the modified EC-SRR is loaded around the antenna and the antenna is oriented so as to take the measurements for the E-plane. Following the same procedure as above the values for gain is recorded. For the second case the antenna without metamaterials is measured the results of the normalized again are plotted as the function of θ as shown in Fig. 4.31. In conclusion, the antenna radiation characteristics were successfully altered and the metamaterials improved the gain of the antenna. Table 4.3 summarized the important results of key antenna parameters obtained from simulation for three different cases:

1. Case 1: Bow tie antenna
2. Case 2: Bow tie antenna with EC-SRR
3. Case 3: Bow tie antenna with modified EC-SRR

Table 4.3: Summary of key simulation results for the three different antenna configurations.

Case #	Resonant Frequency (GHz)	Bandwidth (MHz)	Gain in dB at resonant frequency	Directivity in dB for $\phi = 0$ at Resonant Frequency
1	1.22	230	1.802	1.75
2	1.28	245	2.566	3.16
3	1.32	230	2.824	3.29

The simulation results are considered to be ideal in comparison with measured results for two reasons: the structure of the realized antenna is much different as it still consists of two metal layers instead of one as simulated, the fabrication tolerance of split between the rings and the metal posts impact the performance as they directly affect the resistivity of the structure.

Table 4.4: Measured results of the antenna gain for $\phi = 0$ with and without metamterials.

Parameter	Antenna	Antenna with metamaterials
Normalized gain at $\theta = 0^\circ$	0.36	0.5
Normalized gain at $\theta = 90^\circ$	0.45	0.92

The results indicate the desired performance and design specifications. The summary of this work with and the inferences drawn and further improvements to the existing design are discussion in the conclusion section that follows.

CHAPTER 5: CONCLUSIONS

5.1 Summary of Antenna Design

In this thesis, a comprehensive study of dipole antennas with a major focus on broadband dipoles is undertaken. Some of the common broadband dipole topologies are investigated. The bow-tie antenna is chosen for its robustness and ease in fabrication. Two triangular metal layers on a two sided copper clad FR-4 board connected with vias is made to operate as antenna. The antenna is designed on the X-Y plane with a gap between the feed equal to 5 mm. A coaxial feed is used and the match between the antenna and excitation is achieved by including the feed as within the radiating structure of the antenna. The changes in length of the antenna and the taper angle affected the changed in the antenna parameters. The antenna is optimized to achieve resonance at 1.22 GHz. Upon simulation the antenna is found to have good match with the source and less return loss in the bandwidth. The percentage bandwidth is equal to 19% justifying the its classification as a broadband dipole antenna.

The antenna radiation pattern is broadside and omni-directional as is the case with typical dipole antennas. In order to achieve selective directivity and gain one option is to design an antenna array consisting of multiple bow tie elements. This would mean the requirement of more space on the plane of the antenna, need for power splitters/dividers as feed and matching networks. This is avoided by using a simple technique involving metamaterials to achieve directional propagation. The introduction of a ground plane as a reflector is another means to achieve directional propagation however, it reduces the overall gain of the antenna which makes the use of loading of metamaterials an effective and efficient solution.

5.2 Summary of Metamaterial design

The work involved the design of two types of metamaterial structures used with the antenna to achieve selective directivity and improved gain. Split ring resonators fall under the class of metamaterials known as metaresonators. The concentric rings of appropriate dimensions and splits between them on a substrate form an unit cell. The dimension of an unit cell is designed to be equal to 20 mm which is much less $\frac{\lambda}{10}$ at the resonant frequency. The structure has strong negative permeability at 1.2 GHz.

The second structure was two sided unit cell consisting of edge coupled split ring on one side and metal posts on the other. The modified variation utilizes the electric field components in the near field and the electric field in the near field of the antenna interacts with the metal post resulting in additional capacitance. This topology provides additional degree of freedom that is useful in shifting the resonance of the structure. The first and second version of the edge coupled split ring resonators are used with the antenna and results obtained show directional radiation pattern for the case in which antenna is used with any one of these structures.

5.3 Summary of antenna with metamaterials

The loading of the antenna with metamaterials modifies the antenna far field parameters significantly. The metamaterial array is used to successfully suppress radiation in the direction of the H-plane of the antenna. The metamaterial arrays are excited by the magnetic field of the antenna resulting in negative mu for the overall structure at 1.2 GHz. The directivity is increased in both cases by 95% and gain increased by 40% in the presence of metamaterials around the antenna. The traditional omni-directional radiation pattern was changed to directional radiation pattern with improved efficiency in the E-plane of the antenna compared to the H-plane. This solution overcomes the need for an antenna array to achieve directional propagation.

REFERENCES

[1] S. F. Unversity, "Emspectrum." https://goo.gl/GBtAaZ, 2017.

[2] Qualcomm, "The evolution of mobile technologies." https://www.qualcomm.com/media/documents/files/the-evolution-of-mobile-technologies-1g-to-2g-to-3g-to-4g-lte.pdf, 2014.

[3] I. T. Union, "ICT Facts and Figures 2017." https://www.itu.int/en/ITU-D/Statistics/Documents/facts/ICTFactsFigures2017.pdf, 2017.

[4] K. A. Nordrum and I. Spectrum, "Everything you need to know about 5G." https://spectrum.ieee.org/video/telecom/wireless/everything-you-need-to-know-about-5g, 2017. [Online; accessed 11-October-2017].

[5] S. Koulouridis and J. L. Volakis, "Non-foster circuits for small broadband antennas," *2009 IEEE Antennas and Propagation Society International Symposium*, pp. 1–4, 2009.

[6] V. G. Veselago, "The electrodynamics of substances with simultaneously negative values of ϵ and μ," *Soviet Physics Uspekhi*, vol. 10, no. 4, pp. 509–514, 1968.

[7] J. B. Pendry, A. J. Holden, D. J. Robbins, and W. J. Stewart, "Magnetism from conductors and enhanced nonlinear phenomena," *IEEE Transactions on Microwave Theory and Techniques*, vol. 47, pp. 2075–2084, 1999.

[8] E. R. Brown, C. D. Parker, and E. Yablonovitch, "Radiation properties of a planar antenna on a photonic-crystal substrate," *Journal of Optical Society of America B*, vol. 10, no. 2, pp. 404–407, 1993.

[9] A. Dadgarpour, B. Zarghooni, B. S. Virdee, and T. A. Denidni, "High-gain end-fire bow-tie antenna using artificial dielectric layers," *IET Microwaves, Antennas & Propagation*, vol. 9, no. 12, pp. 1254–1259, 2015.

[10] S. Ehoch, G. Tayeb, P. Sabouroux, N. Guérin, and P. Vincent, "A metamaterial for directive emission," *Physics Review Letters*, vol. 89, no. 21, pp. 213902–1–213902–4, 2002.

[11] B. I. Wu, W. Wang, J. Pacheco, X. Chen, T. Grzegorczyk, and J. A. Kong, "A study of using metamaterials as antennna substrate to enhance gain," *Progress in Electromagnetics Research*, vol. 51, pp. 295–328, 2005.

[12] R. W. Ziolkowski, "Metamaterial-inspired configurations to enhance the directivity of electrically small antennas," *Progress in Electromagnetics Research*, vol. 51, pp. 295–328, 2005.

[13] C. A. Balanis, *Antenna Theory, Analysis and Design*. Hoboken, NJ: John Wiley & Sons Inc, 2005.

[14] R. S. Adams, "Antennas, ECGR 5121," Fall 2016. Lectures on Broadband Dipoles.

[15] W. L. Stutzman and G. A. Thiele, *Antenna Theory and Design*. Hoboken, NJ: John Wiley & Sons Inc, 1998.

[16] G. H. Brown and O. M. W. Jr, "Experimentally determined impedance characteristics of cylindrical antennas," *Proc. IRE*, vol. 33, pp. 257–262, 1945.

[17] C. A. Balanis, *Advanced Engineering Electromagnetics*. Hoboken, NJ: John Wiley & Sons Inc, 2012.

[18] N. Engheta and R. W. Ziolkowski, *Electromagnetic Metamaterials: Physics and Engineering Explorations*. Hoboken, NJ: John Wiley & Sons Inc, 2006.

[19] C. Caloz and T. Itoh, *Electromagnetic Metamaterials, Transmission Line Theory and Microwave Applications*. Hoboken, NJ: John Wiley & Sons Inc, 2006.

[20] I. V. Lindell, S. A. Tretyakov, K. Nikoskinen, and S. Iivonen, "Bw media–media with negative parameters, capable of supporting backward waves," *Microwave and Optical Technology Letters*, vol. 31, no. 2, pp. 129–133, 2001.

[21] J. A. Kong, B.-I. Wu, and Y. Zhang, "A unique lateral displacement of a gaussian beam transmitted through a slab with neagative permittivity and permeability," *Microwave and Optical Technology Letters*, vol. 31, no. 2, pp. 129–133, 2001.

[22] D. Smith, D.Schurig, and J. B. Pendry, "Negative refraction of modulated electromagnetic waves," *Applied Physics Letters*, vol. 81, no. 15, pp. 2713–2715, 2002.

[23] M. W. McCall, A. Lakhtakia, and W. S. Weiglhofer, "The negative index of refraction demystified," *European Journal of Physics*, vol. 23, no. 3, pp. 353–359, 2002.

[24] P. Markoš and C. M. Soukoulis, "Negative refraction of modulated electromagnetic waves," *Physical Review E*, vol. 65, no. 036622, pp. 036622–1–036622–8, 2002.

[25] A. L. Pokrovsky and A. L. Efros, "Electrodynamics of metallic photonic crystals and the proble of left-handed materials," *Physical Review Letters*, vol. 89, no. 9, pp. 93901–1–93901–4, 2002.

[26] N. Garcia and M. Nieto-Vesperinas, "Is there an experimental verification of a negative index of refraction yet?," *Optics Letters*, vol. 27, no. 11, pp. 885–887, 2002.

[27] P. M. Valanju, R. M. Walser, and A. P. Valanju, "Wave refraction in negative index media: Always positive and very inhomogeneous," *Physics Review Letters*, vol. 88, no. 18, pp. 187401–1–187401–4, 2002.

[28] B. A. Munk, *Metamaterials: Critique and Alternatives*. Hoboken, NJ: John Wiley & Sons Inc, 2008.

[29] R. S. Adams, "Advanced electromagnetics, ECGR 5123," Spring 2017. Lectures on Wave Propagation.

[30] K. Aydin, I. Bulu, K. Guven, M. Kafesaki, C. M. Soukouis, and E. Ozbay, "Investigation of magnetic resonances for different split-ring resonator parameters and designs," *New Journal of Physics*, vol. 7, 2005.

[31] C. H. Papas and R. King, "Radiation from wide-angle concial antennas fed by a coaxial line," *Proc. IRE*, vol. 39, 1949.

[32] Z. Szabó, G.-H. Park, R. Hedge, and E.-P. Li, "A unique extraction of metamaterial parameters based on kramers-kronig relationship," *IEEE Transactions on Microwave Theory and Techniques*, vol. 58, no. 10, 2010.

VITA

Ajay Naik is a graduate student pursuing Master in Electrical Engineering at University of North Carolina at Charlotte. He hails from Sirsi in southern part of India from the state of Karnataka. He has a bachelor's in engineering majoring in electronics and communication from New Horizon College of Engineering, Bengaluru, India. His research interests are Antennas, Metamaterials, RFIC and Microwave Circuits.